Chapter 2

Magnetic Materials and Their Characteristics

Introduction

The magnetic material is the paramount player in the design of magnetic components. The magnetics design engineer has three standard words when making the normal design trade-off study: cost, size, and performance. He will be happy to stuff any two into the bag. The magnetics engineer is now designing magnetic components that operate from below the audio range to the megahertz range. He is normally asked to design for maximum performance, with the minimum of his parasitic friends' capacitance and leakage inductance. Today, the magnetic materials the engineer has to work with are silicon steel, nickel iron (permalloy), cobalt iron (permendur), amorphous metallic alloys, and ferrites. These also have spin-off material variants, such as moly-permalloy powder, sendust powder, and iron powder cores. From this group of magnetic materials, the engineer will make trade-offs with the magnetic properties for his design. These properties are: saturation B_s, permeability μ, resistivity ρ (core loss), remanence B_r, and coercivity H_c.

Saturation

A typical hysteresis loop of a soft magnetic material is shown in Figure 2-1. When a high magnetizing force is encountered, a point is reached where further increase in, H, does not cause useful increase in, B. This point is known as the saturation point of that material. The saturation flux density, B_s, and the required magnetizing force, H_s, to saturate the core are shown with dashed lines.

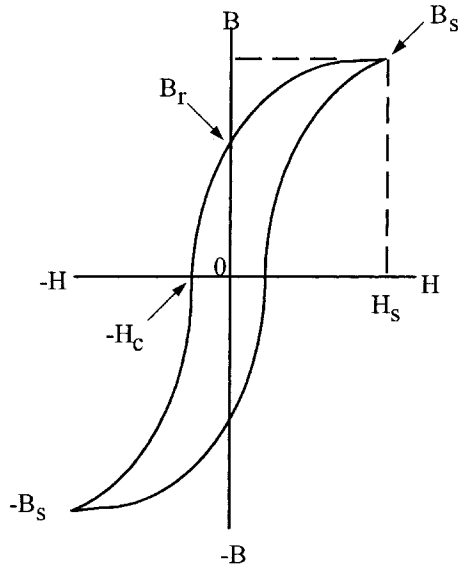

Figure 2-1. Typical B-H or Hysteresis Loop of a Soft Magnetic Material.

Remanence Flux, B_r, and Coercivity H_c

In Figure 2-1 the hysteresis loop clearly shows the remanence flux density, B_r. The remanence flux is the polarized flux remaining in the core after the excitation has been removed. The magnetizing force, $-H_c$, is called coercivity. It is the amount of magnetizing force required to bring the remanence flux density back to zero.

Permeability, μ

The permeability of a magnetic material is a measure of the ease in magnetizing the material. Permeability, μ, is the ratio of the flux density, B, to the magnetizing force, H.

$$\mu = \frac{B}{H}, \quad \text{[permeability]} \quad \text{[2-1]}$$

The relationship between B and H is not linear, as shown in the hysteresis loop in Figure 2-1. Then, it is evident that the ratio, B/H, (permeability), also varies. The variation of permeability with flux density, B, is shown in Figure 2-2. Also, it shows the flux density at which the permeability is at a maximum.

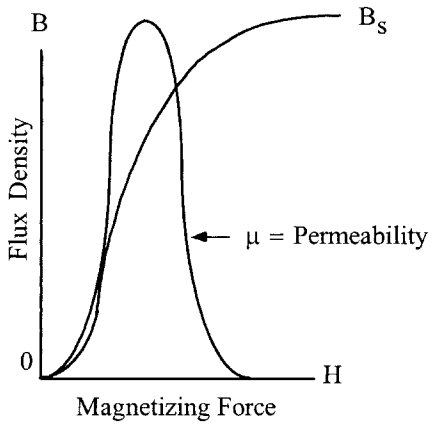

Figure 2-2. Variation in Permeability μ with B and H.

Hysteresis Loss, Resistivity, ρ, (core loss)

The enclosed area within the hysteresis, shown in Figure 2-1, is a measure of the energy lost in the core material during that cycle. This loss is made up in two components: (1) the hysteresis loss and (2) eddy current loss. The hysteresis loss is the energy loss when the magnetic material is going through a cycling state. The eddy current loss is caused when the lines of flux pass through the core, inducing electrical currents in it. These currents are called eddy currents and produce heat in the core. If the electrical resistance of the core is high, the current will be low; therefore, a feature of low-loss material is high electrical resistance. In the norm, when designing magnetic components, the core loss is a major design

factor. Core loss can be controlled by selecting the right material and thickness. Selecting the correct material, and operating within its limits, will prevent overheating that could result in damage to the wire insulation and/or the potting compound.

Introduction to Silicon Steel

Silicon steel was one of the first alloys to be used in transformers and inductors. It has been greatly improved over the years and is probably, pound for pound, the most, widely used magnetic material. One of the drawbacks in using steel in the early years was, as the material became older, the losses would increase. With the addition of silicon to the steel, the advantages were twofold: it increased the electrical resistivity, therefore reducing the eddy current losses, and it also improved the material's stability with age.

Silicon steel offers high saturation flux density, a relatively good permeability at high flux density, and a moderate loss at audio frequency. One of the important improvements made to the silicon steel was in the process called cold-rolled, grain-oriented, AISI type M6. This M6 grain-oriented steel has exceptionally low losses and high permeability. It is used in applications requiring high performance and the losses will be at a minimum.

Introduction to Thin Tape Nickel Alloys

High permeability metal alloys are based primarily on the nickel-iron system. Although Hopkinson investigated nickel-iron alloys as early as 1889, it was not until the studies by Elmen, starting in about 1913, on properties in weak magnetic fields and effects of heat-treatments, that the importance of the Ni-Fe alloys was realized. Elmen called his Ni-Fe alloys, "Permalloys," and his first patent was filed in 1916. His preferred composition was the 78Ni-Fe alloy. Shortly after Elmen, Yensen started an independent investigation that resulted in the 50Ni-50Fe alloy, "Hipernik," which has lower permeability and resistivity but higher saturation than the 78-Permalloy, (1.5 tesla compared to 0.75 tesla), making it more useful in power equipment.

Improvements in the Ni-Fe alloys were achieved by high temperature anneals in hydrogen atmosphere, as first reported by Yensen. The next improvement was done by using grain-oriented material and annealing it, in a magnetic field, which was also in a hydrogen atmosphere. This work was done by Kelsall and Bozorth. Using these two methods, a new material, called Supermalloy, was achieved. It has a higher permeability, a lower coercive force, and about the same flux density as 78-Permalloy. Perhaps the most important of these factors is the magnetic anneal, which, not only increases permeability, but also provides a "square" magnetization curve, important in high frequency power conversion equipment.

In order to obtain high resistance, and therefore lower core losses for high frequency applications, two approaches have been followed: (1) modification of the shape of metallic alloys and (2) development of magnetic oxides. The result was the development of thin tapes and powdered alloys in the 1920's, and thin films in the 1950's. The development of thin film has been spurred by the requirements of aerospace, power conversion electronics from the mid 1960's to the present.

The Ni-Fe alloys are available in thicknesses of 2 mil, 1 mil, 0.5 mil, 0.25 and 0.125 mil. The material comes with a round or square B-H loop. This gives the engineer a wide range of sizes and configurations from which to select for a design. The iron alloy properties for some of the most popular materials are shown in Table 2-1. Also, given in Table 2-1, is the Figure number for the B-H loop of each of the magnetic materials.

Table 2-1 Magnetic Properties for Selected Iron Alloys Materials.

Iron Alloy Material Properties								
Material Name	Composition	Initial Permeability μ_i	Flux Density Tesla B_s	Curie Temp. °C	dc, Coercive Force, Hc Oersteds	Density grams/cm^3 δ	Weight Factor x	Typical B-H Loop Figures
Silicon	3% Si 97% Fe	1.5 K	1.5-1.8	750	0.4-0.6	7.63	1.000	(2-3)
Supermendur*	49% Co 49% Fe 2% V	0.8 K	1.9-2.2	940	0.15-0.35	8.15	1.068	(2-4)
Orthonol	50% Ni 50% Fe	2 K	1.42-1.58	500	0.1-0.2	8.24	1.080	(2-5)
Permalloy	79% Ni 17% Fe 4% Mo	12 K-100 K	0.66-0.82	460	0.02-0.04	8.73	1.144	(2-6)
Supermalloy	78% Ni 17% Fe 5% Mo	10 K-50 K	0.65-0.82	460	0.003-0.008	8.76	1.148	(2-7)

* Field Anneal.

x Silicon has unity weight factor.

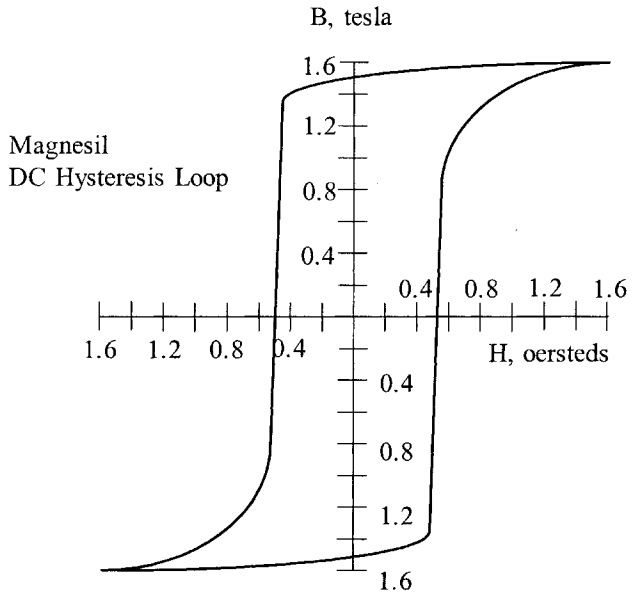

Figure 2-3. Silicon B-H Loop: 97% Fe 3% Si.

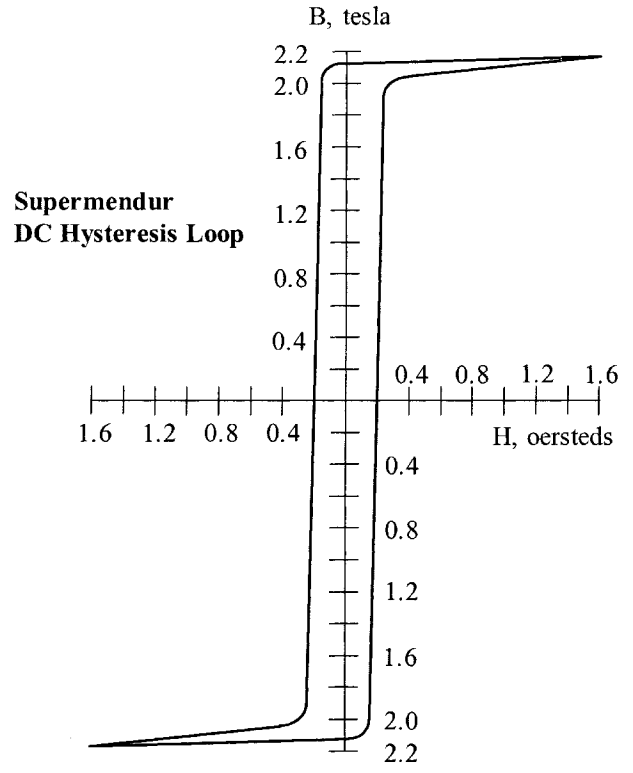

Figure 2-4. Supermendur B-H Loop: 49% Fe 49% Co 2% V.

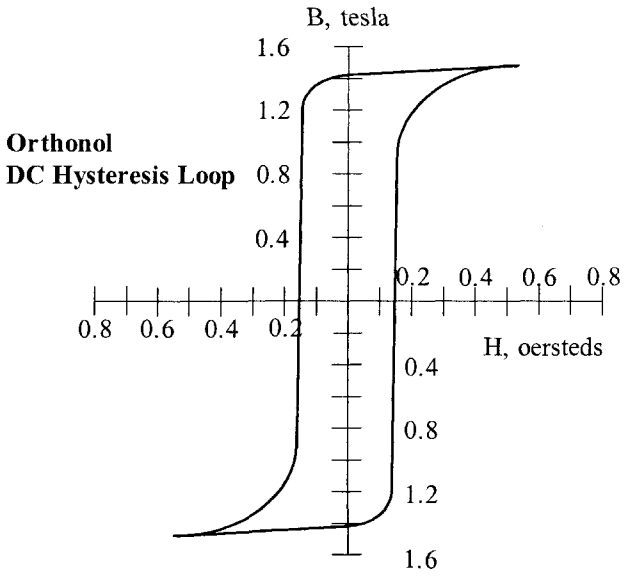

Figure 2-5. Orthonol B-H loop: 50% Fe 50% Ni.

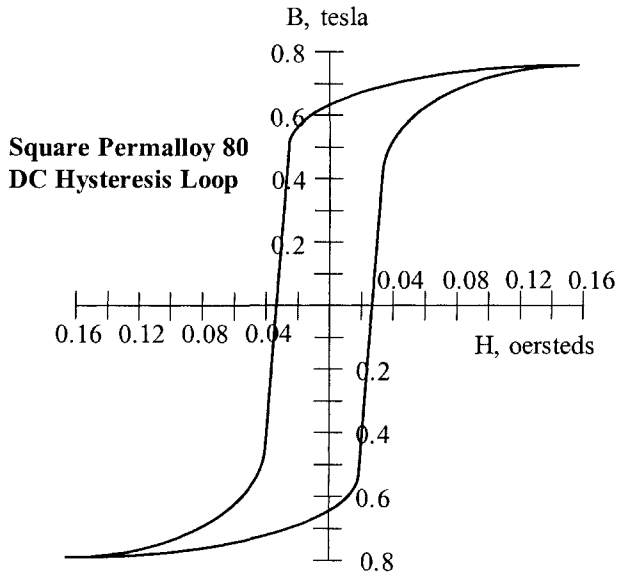

Figure 2-6. Square Permalloy 80 B-H loop: 79% Ni 17% Fe 4% Mo.

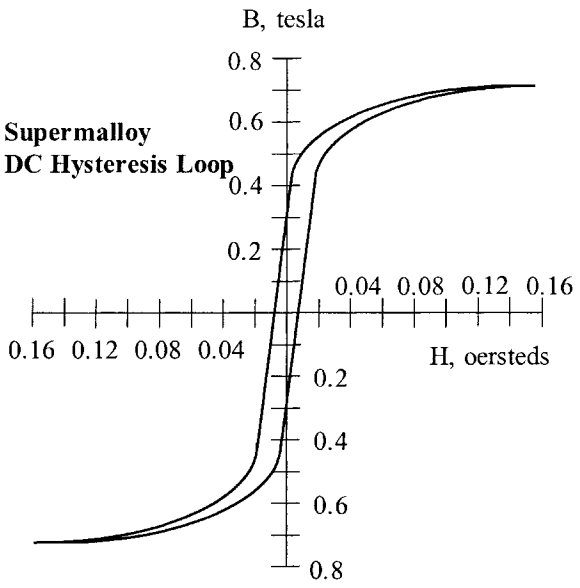

Figure 2-7. Supermalloy B-H Loop: 78% Ni 17% Fe 5% Mo.

Introduction to Metallic Glass

The first synthesis of a metallic glass drawing wide attention among material scientists, occurred in 1960. Klement, Willens and Duwez reported that a liquid, AuSi alloy, when rapidly quenched to liquid nitrogen temperature, would form an amorphous solid. It was twelve years later that Chen and Polk produced ferrous-based metallic glasses in useful shapes with significant ductility. Metallic glasses have since survived the transition from laboratory curiosities to useful products, and currently are the focus of intensive technological and fundamental studies.

Metallic glasses are generally produced, by liquid quenching, in which a molten metal alloy is rapidly cooled, at rates on the order of 10^5 degrees/sec., through the temperature at which crystallization normally occurs. The basic difference between crystalline (standard magnetic material) and glassy metals is in their atomic structures. Crystalline metals are composed of regular, three-dimensional arrays of atoms which exhibit long-range order. Metallic glasses do not have long-range structural order. Despite their structural differences, crystalline and glassy metals of the same compositions exhibit nearly the same densities.

The electrical resistivities of metallic glasses are much larger, (up to three times higher), than those of crystalline metals of similar compositions. The magnitude of the electrical resistivities and their temperature coefficients in the glassy and liquid states are almost identical.

Metallic glasses are quite soft magnetically. The term, "soft," refers to a large response of the magnetization to a small-applied field. A large magnetic response is desirable in such applications as transformers and inductors. The obvious advantages of these new materials are in high frequency applications with their high induction, high permeability and low core loss.

There are four amorphous materials that have been used in high frequency applications: 2605SC, 2714A, 2714AF and Vitroperm 500F. Material 2605SC offers a unique combination of high resistivity, high saturation induction, and low core loss, making it suitable for designing high frequency dc inductors. Material 2714A is a cobalt material that offers a unique combination of high resistivity, high squareness ratio B_r/B_S, and very low core loss, making it suitable for designing high frequency aerospace transformers and mag-amps. The Vitroperm 500F is an iron based material with a saturation of 1.2 tesla and is well-suited for high frequency transformers and gapped inductors. The high frequency core loss for the nanocrystal 500F is lower than some ferrite, even operating at a high flux density. The amorphous properties for some of the most popular materials are shown in Table 2-2. Also, given in Table 2-2, is the Figure number for the B-H loop of each of the magnetic materials.

Table 2-2. Magnetic Properties for Selected Amorphous Materials.

Amorphous Material Properties								
Material Name	Major Composition	Initial Permeability μ_i	Flux Density Tesla B_s	Curie Temperature °C	dc, Coercive Force, Hc Oersteds	Density grams/cm^3 δ	Weight Factor x	Typical B-H Loop Figures
2605SC	81% Fe 13.5% B 3.5% Si	1.5K	1.5-1.6	370	0.4-0.6	7.32	0.957	(2-8)
2714A	66% Co 15% Si 4% Fe	0.8K	0.5-0.65	205	0.15-0.35	7.59	0.995	(2-9)
2714AF	66% Co 15% Si 4% Fe	2K	0.5-0.65	205	0.1-0.2	7.59	0.995	(2-10)
Nanocrystal Vitroperm 500F*	73.5% Fe 1% Cu 15.5% Si	30K-80K	1.0-1.2	460	0.02-0.04	7.73	1.013	(2-11)

* Vitroperm is the trademark of Vacuumschmelze.

x Silicon has a unity weight factor. See Table 2-1.

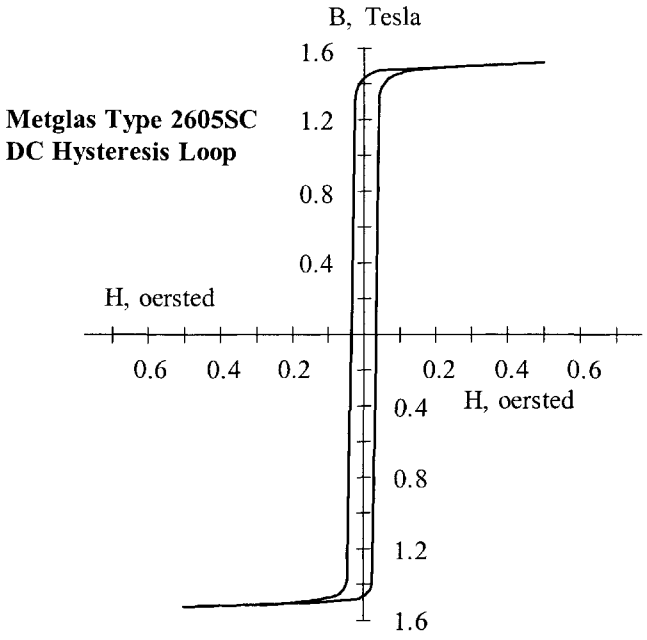

Figure 2-8. Amorphous 2605SC B-H Loop: 81% Fe 13.5% B 3.5% Si.

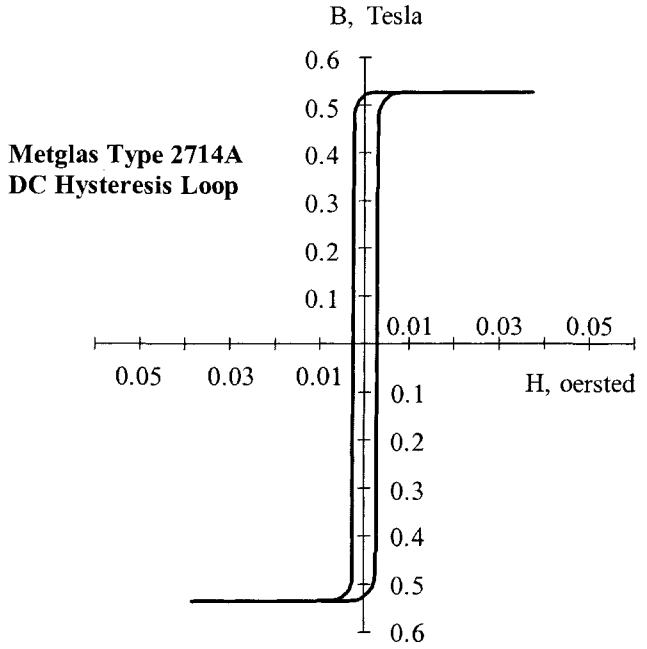

Figure 2-9. Amorphous 2714A B-H Loop: 66% Co 15% Si 4% Fe.

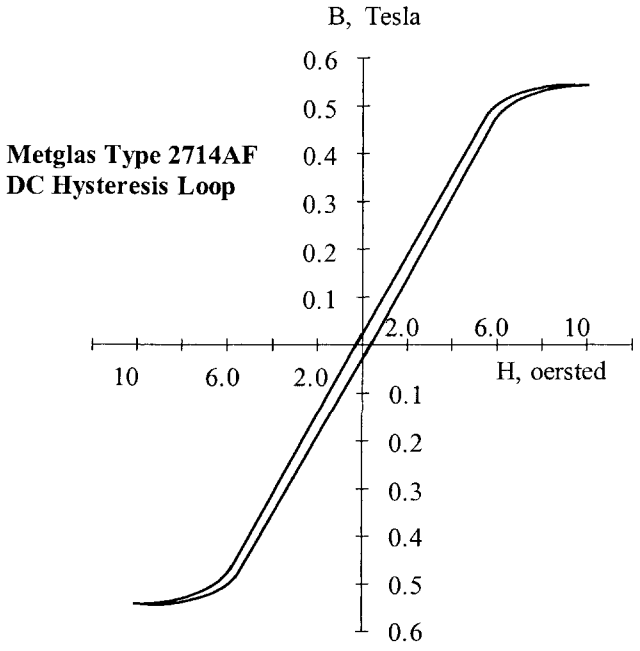

Figure 2-10. Amorphous 2714AF B-H Loop: 66% Co 15% Si 4% Fe.

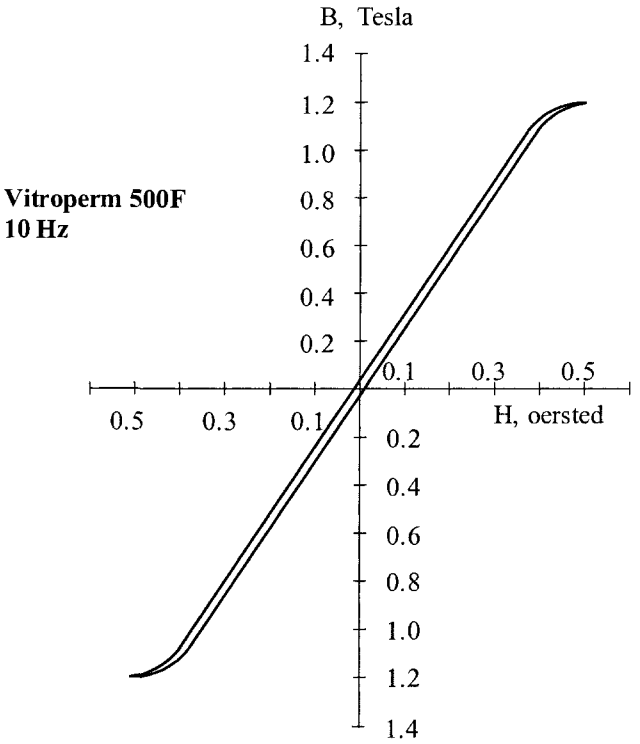

Figure 2-11. Vitroperm 500F B-H loop: 73.5% Fe 15.5% Si 1% Cu.

Introduction to Soft Ferrites

In the early days of electrical industry, the need for the indispensable magnetic material was served by iron and its magnetic alloys. However, with the advent of higher frequencies, the standard techniques of reducing eddy current losses, (using laminations or iron powder cores), was no longer efficient or cost effective.

This realization stimulated a renewed interest in "magnetic insulators," as first reported by S. Hilpert in Germany, in 1909. It was readily understood that, if the high electrical resistivity of oxides could be combined with desired magnetic characteristics, a magnetic material that was particularly well-suited for high frequency operation would result.

Research to develop such a material was being performed by scientists in various laboratories all over the world, such as V. Kato, T. Takei, and N. Kawai in the 1930's in Japan, and by J. Snoek of the Philips' Research Laboratories in the period 1935-1945 in The Netherlands. By 1945, Snoek had laid down the basic fundamentals of the physics and technology of practical ferrite materials. In 1948, the Neel Theory of ferromagnetism provided the theoretical understanding of this type of magnetic material.

Ferrites are ceramic, homogeneous materials composed of oxides; iron oxide is their main constituent. Soft ferrites can be divided into two major categories; manganese-zinc and nickel-zinc. In each of these categories, changing the chemical composition, or manufacturing technology, can manufacture many different Mn-Zn and Ni-Zn material grades. The two families of Mn-Zn and Ni-Zn ferrite materials complement each other, and allow the use of soft ferrites from audio frequencies to several hundred megahertz. Manufacturers do not like to handle manganese-zinc in the same area, or building with nickel-zinc, because one contaminates the other, which leads to poor performance yields. The basic difference between Manganese-Zinc and Nickel-Zinc is shown in Table 2-3. The biggest difference is Manganese-Zinc has a higher permeability and Nickel-Zinc has a higher resistivity. Shown in Table 2-4 are some of the most popular ferrite materials. Also, given in Table 2-4, is the Figure number for the B-H loop of each of the materials.

Table 2-3. Comparing Manganese-Zinc and Nickel-Zinc Basic Properties.

Basic Ferrite Material Properties					
Materials	Initial Permeability μ_i	Flux Density B_{max} Tesla	Curie Temperature, °C	dc, Coercive Force, H_c Oersteds	Resistivity Ω - cm
Manganese Zinc	750-15 K	0.3-0.5	100-300	0.04-0.25	10-100
Nickel Zinc	15-1500	0.3-0.5	150-450	0.3-0.5	10^6

Manganese-Zinc Ferrites

This type of soft ferrite is the most common, and is used in many more applications than the nickel-zinc ferrites. Within the Mn-Zn category, a large variety of materials are possible. Manganese-zinc ferrites are primarily used at frequencies less than 2 MHz.

Nickel-Zinc Ferrites

This class of soft ferrite is characterized by its high material resistivity, several orders of magnitude higher than Mn-Zn ferrites. Because of its high resistivity, Ni-Zn ferrite is the material of choice for operating from 1-2 MHz to several hundred megahertz.

The material permeability, μ_m, has little influence on the effective permeability, μ_e, when the gap dimension is relatively large, as shown in Table 2-5.

Table 2-4. Magnetic Properties for Selected Ferrite Materials.

Ferrites Material Properties							
*Magnetics Material Name	Initial Permeability μ_i	Flux Density Tesla B_s@15 Oe	Residual Flux Tesla B_r	Curie Temperature °C	dc, Coercive Force, Hc Oersteds	Density grams/cm^3 δ	Typical B-H Loop Figures
K	1500	0.48T	0.08T	>230	0.2	4.7	(2-12)
R	2300	0.50T	0.12T	>230	0.18	4.8	(2-13)
P	2500	0.50T	0.12T	>230	0.18	4.8	(2-13)
F	5000	0.49T	0.10T	>250	0.2	4.8	(2-14)
W	10,000	0.43T	0.07T	>125	0.15	4.8	(2-15)
H	15,000	0.43T	0.07T	>125	0.15	4.8	(2-15)
*Magnetics, a Division of Spang & Company							

Table 2-5. Permeability, and its Effect on Gapped Inductors.

Comparing Material Permeabilities					
*Material	μ_m	Gap, inch	Gap, cm	**MPL, cm	μ_e
K	1500	0.04	0.101	10.4	96
R	2300	0.04	0.101	10.4	98
P	2500	0.04	0.101	10.4	99
F	3000	0.04	0.101	10.4	100
*The materials are from Magnetics, a Division of Spang and Company					
**Core , ETD44					

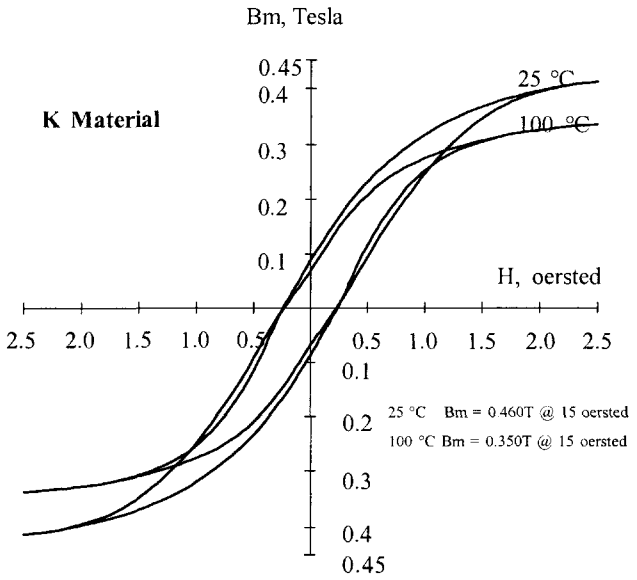

Figure 2-12. Ferrite B-H loop, K Material at 25 and 100 °C.

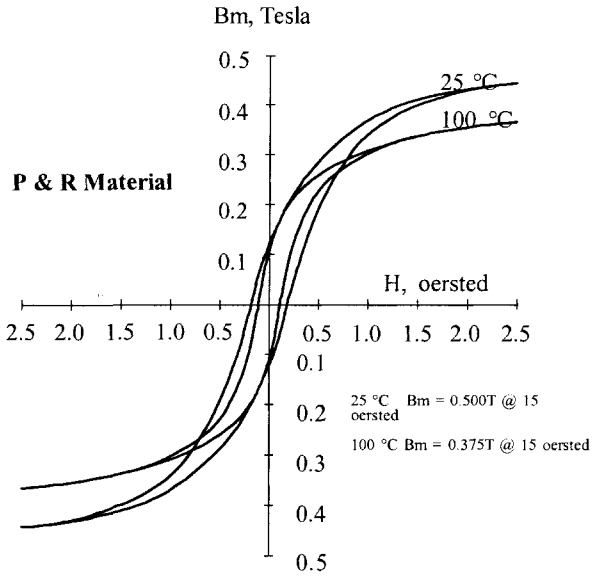

Figure 2-13. Ferrite B-H loop, P & R Material at 25 and 100 °C.

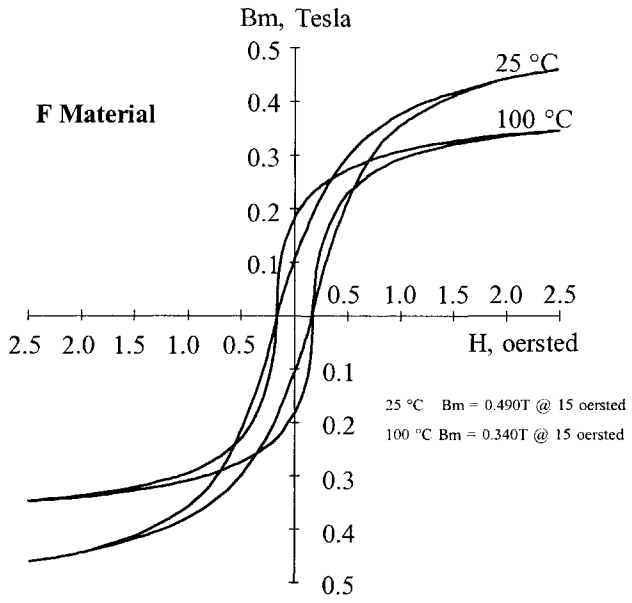

Figure 2-14. Ferrite B-H loop, F Material at 25 and 100 ° C.

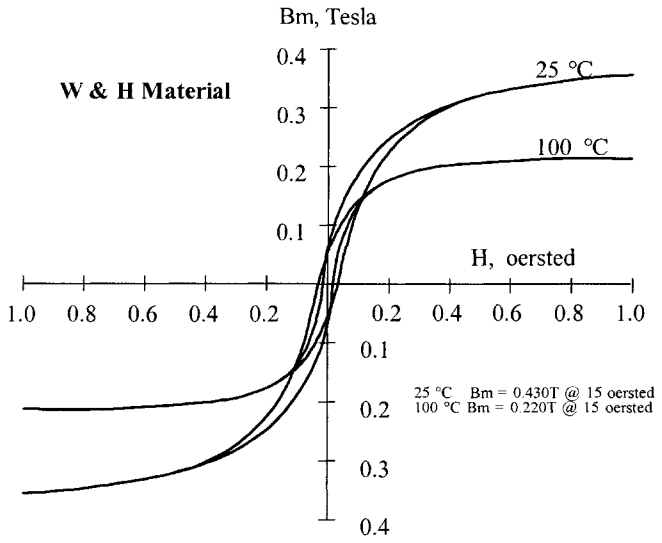

Figure 2-15. Ferrite B-H loop, W & H Material at 25 and 100 ° C.

Ferrite Cross Reference

The cross-reference, Table 2-6, has been put together using some of the leading ferrite manufacturers. The ferrite materials have been organized and referenced under Magnetics materials. This is because Magnetics has one of the broadest lines of standard ferrite materials.

Table 2-6. Ferrite Materials, Manufacturers' Cross-Reference.

Ferrite Material Cross Reference							
Permeability	1500	2300	2500	3000	5000	10000	15000
Application	Power	Power	Power	Power	Filter	Filter	Filter
Manufacturer's	Material Designation						
Magnetics	1 K	2 R	3 P	F	J	W	H
Ferroxcube	3F35	3F3	3C94	3C81	3E27	3E5	3E7
Permeability, μ_i	1400	2000	2300	2700	6000	10000	15000
Fair-Rite			78		75	76	
Permeability, μ_i			2300		5000	10000	
Siemens	N49	N87	N67	T41	T35	T38	T46
Permeability, μ_i	1300	2200	2100	3000	6000	10000	15000
TDK Corp.	PC50	PC40	PC44	H5A	HP5	H5C2	H5C3
Permeability, μ_i	1400	2300	2400	3300	5000	10000	15000
MMG		F44	F5	F5C	F-10	F-39	
Permeability, μ_i		1900	2000	3000	6000	10000	
Ceramic Mag	MN67	MN80	MN80	MN8CX	MN60	MC25	MC15K
Permeability, μ_i	1000	2000	2000	3000	6000	10000	15000
Tokin		HBM	B25	B3100	H5000	H12000	
Permeability, μ_i							
Ferrite Int.	TSF-5099	TSF-7099	TSF-7070	TSF-8040	TSF-5000	TSF-010K	
Permeability, μ_i	2000	2000	2200	3100	5000	10000	

1. High Frequency power material 250 kHz & up.
2. Lowest loss at 80°-100°C, 25 kHz to 250 kHz.
3. Lowest loss at 60°C-80°C.

Introduction to Molypermalloy Powder Cores

The nickel-iron (Ni-Fe) high permeability magnetic alloys (permalloy) were discovered in 1923 and 1927. Permalloy alloys were successfully used in powder cores, greatly contributing to the carrier wave communications of the time.

In the early 1940's, a new material, trademarked Molybdenum Permalloy Powder (MPP), was developed into cores by the Bell Telephone Laboratory and the Western Electric Company. This new material was developed for loading coils, filtering coils, and transformers at audio and carrier frequencies in the telephone facility. The use of such cores has been extended to many industrial and military circuits. The stability of permeability and core losses with time, temperature, and flux level, are particularly important to engineers designing tuned circuits and timing circuits. This new material has given reliable and superior performance over all past powder core materials.

Molybdenum permalloy powder, [2 Molybdenum (Mo)-82 Nickel (Ni)-16 Iron (Fe)], is made by grinding hot-rolled and embrittled cast ingots; then, the alloy is insulated and screened to a fineness of 120 mesh for use in audio frequency applications, and 400 mesh for use at high frequencies.

In the power conversion field, the MPP core has made its greatest impact in switching power supplies. The use of MPP cores and power MOSFET transistors has permitted increased frequency, resulting in greater compactness and weight reduction in computer systems. The power supply is the heart of the system. When the power supply is designed correctly, using a moderate temperature rise, the system will last until it becomes obsolete. In these power systems there are switching inductors, smoothing choke coils, common mode filters, input filters, output filters, power transformers, current transformers and pulse transformers. They cannot all be optimally designed, using MPP cores. But, in some cases, MPP cores are the only ones that will perform in the available space with the proper temperature rise.

Introduction to Iron Powder Cores

The development of compressed iron powder cores as a magnetic material for inductance coils, stemmed from efforts of Bell Telephone Laboratory engineers to find a substitute for fine iron-wire cores. The use of iron powder cores was suggested by Heaviside, in 1887, and again, by Dolezalek in 1900.

The first iron powder cores of commercially valuable properties were described by Buckner Speed, in U.S. Patent No. 1274952, issued in 1918. Buckner Speed and G.W. Elman published a paper in the A.I.E.E. Transactions, "Magnetic Properties of Compressed Powdered Iron," in 1921. This paper describes a

magnetic material, which is well-suited to the construction of cores in small inductance coils and transformers, such as those used in a telephone system. These iron powder cores were made from 80 Mesh Electrolytic Iron Powder. The material was annealed, then, insulated by oxidizing the surface of the individual particles. In this way, a very thin and tough insulation of grains of iron was obtained; this did not break down when the cores were compressed. A shellac solution was applied to the insulated powder as a further insulator and binder. This was how toroidal iron powder cores were manufactured by Western Electric Company until about 1929. Today's iron powder cores are manufactured in much the same way, using highly pure iron powder and a more exotic insulator and binder. The prepared powder is compressed under extremely high pressures to produce a solid-looking core. This process creates a magnetic structure with a distributed air-gap. The inherent high saturation flux density of iron, combined with the distributed air-gap, produces a core material with initial permeability of less than 100, and with high-energy storage capabilities.

The dc current does not generate core loss, but an ac or ripple current does generate core loss. Iron powder material has higher core loss than some other, more expensive, core materials. Most dc-biased inductors have a relatively small percentage of ripple current and, thus, core loss will be minimal. However, core loss will sometimes become a limiting factor in applications with a relatively high percentage of ripple current at very high frequency. Iron powder is not recommended for inductors with discontinuous current or transformers with large ac flux swings.

Low cost, iron powder cores are typically used in today's, low and high frequency power switching conversion applications, for differential-mode, input and output power inductors. Because iron powder cores have such low permeability, a relatively large number of turns are required for the proper inductance, thus keeping the ac flux at a minimum. The penalty for using iron powder cores is usually found in the size and efficiency of the magnetic component.

There are four standard powder materials available for power magnetic devices: Molypermalloy (MPP) Powder Cores with a family of curves, as shown in Figure 2-20; High flux (HF) Powder Cores with a family of curves, as shown in Figure 2-21; Sendust Powder Cores, *(Kool Mμ), with a family of curves, as shown in Figure 2-22; and Iron Powder Cores, with a family of curves, as shown in Figure 2-23. The powder cores come in a variety of permeabilities. This gives the engineer a wide range in which to optimize the design. The powder core properties for the most popular materials are shown in Table 2-7. Also, given in Table 2-7, is the Figure number for the B-H loop of each of the powder core materials. In Table 2-8 is a listing of the most popular permeabilities for each of the powder core materials.

*Trademark of Magnetics Division, Spang and Company.

Table 2-7. Powder Core Material Properties.

Powder Core Material Properties							
Material Name	Composition	Initial Permeability μ_i	Flux Density Tesla B_s	Curie Temperature °C	dc, Coercive Force, Hc Oersteds	Density grams/cm^3 δ	Typical B-H Loop Figures
MPP	80% Ni 20% Fe	14-550	0.7	450	0.3	8.5	(2-16)
High Flux	50% Ni 50% Fe	14 - 160	1.5	360	1	8	(2-17)
Sendust (Kool Mμ)	85% Fe 9% Si 6% Al	26 - 125	1	740	0.5	6.15	(2-18)
Iron Powder	100% Fe	4.0 - 100	0.5 - 1.4	770	5.0 - 9.0	3.3 - 7.2	(2-19)

Table 2-8. Standard Powder Core Permeabilities.

Standard Powder Core Permeabilities				
Powder Material	MPP	High Flux	Sendust (Kool Mμ)	Iron Powder
Initial Permeability, μ_i				
10				X
14	X	X		
26	X	X	X	
35				X
55				X
60	X	X	X	X
75			X	X
90			X	
100				X
125	X	X	X	
147	X	X		
160	X	X		
173	X			
200	X			
300	X			
550	X			

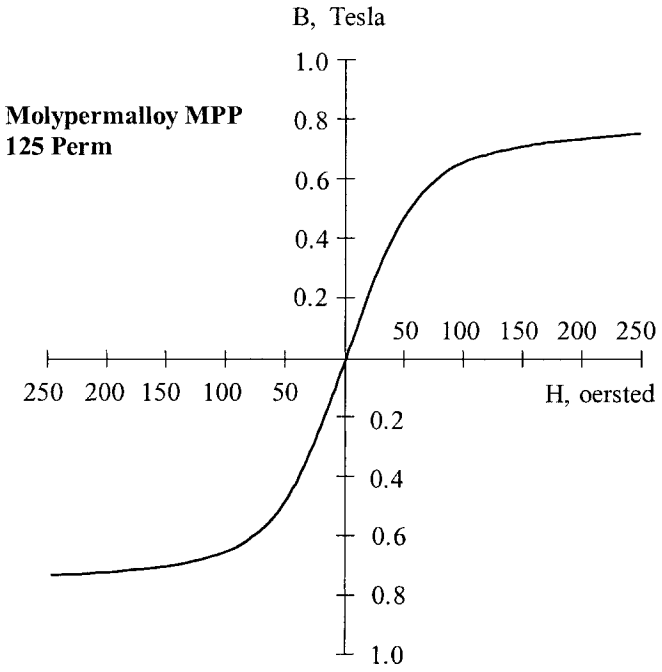

Figure 2-16. Molypermalloy Powder Core, 125 Perm.

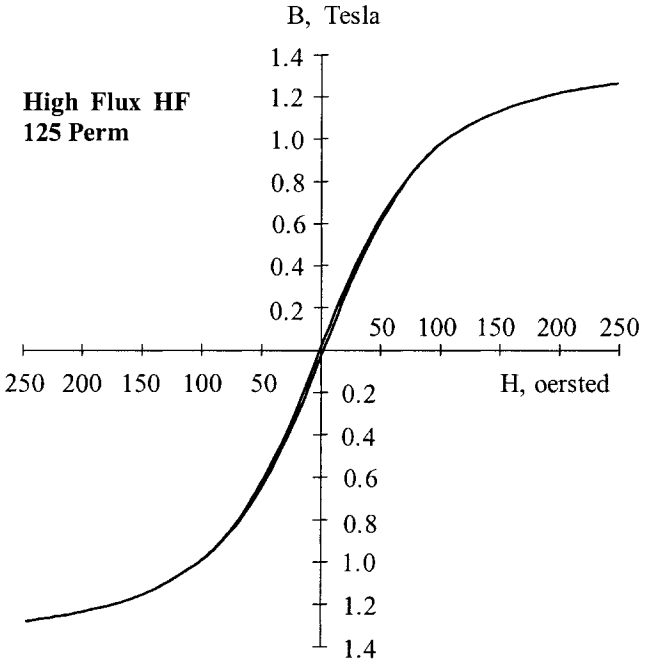

Figure 2-17. High Flux Powder Core, 125 Perm.

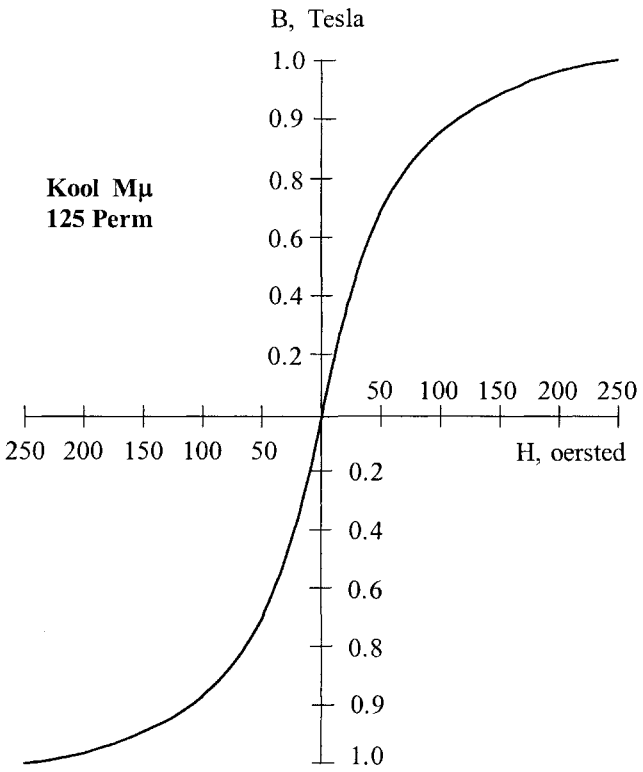

Figure 2-18. Sendust (Kool Mμ) Powder Core, 125 Perm.

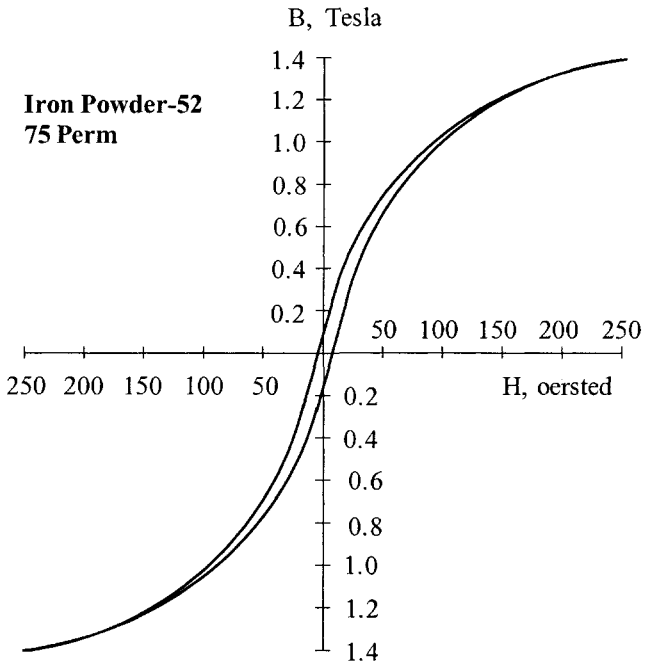

Figure 2-19. Iron Powder (-52) Core, 75 Perm.

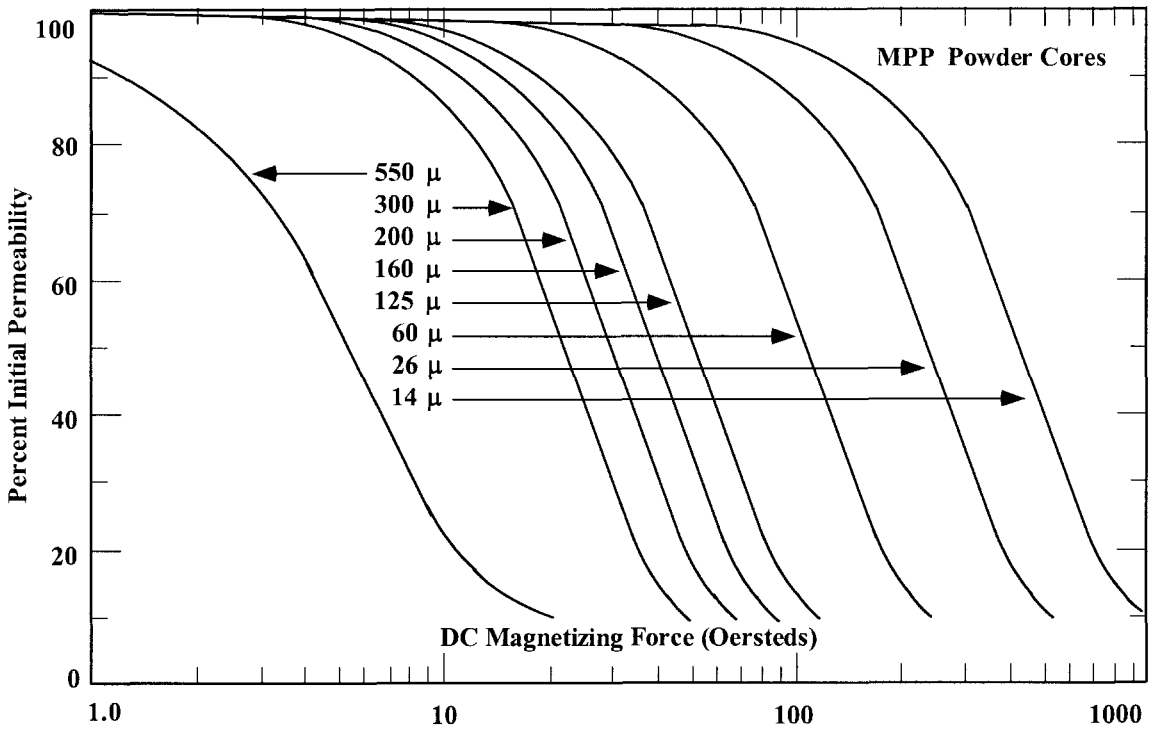

Figure 2-20. Permeability Versus dc Bias for Molypermalloy Powder Cores.

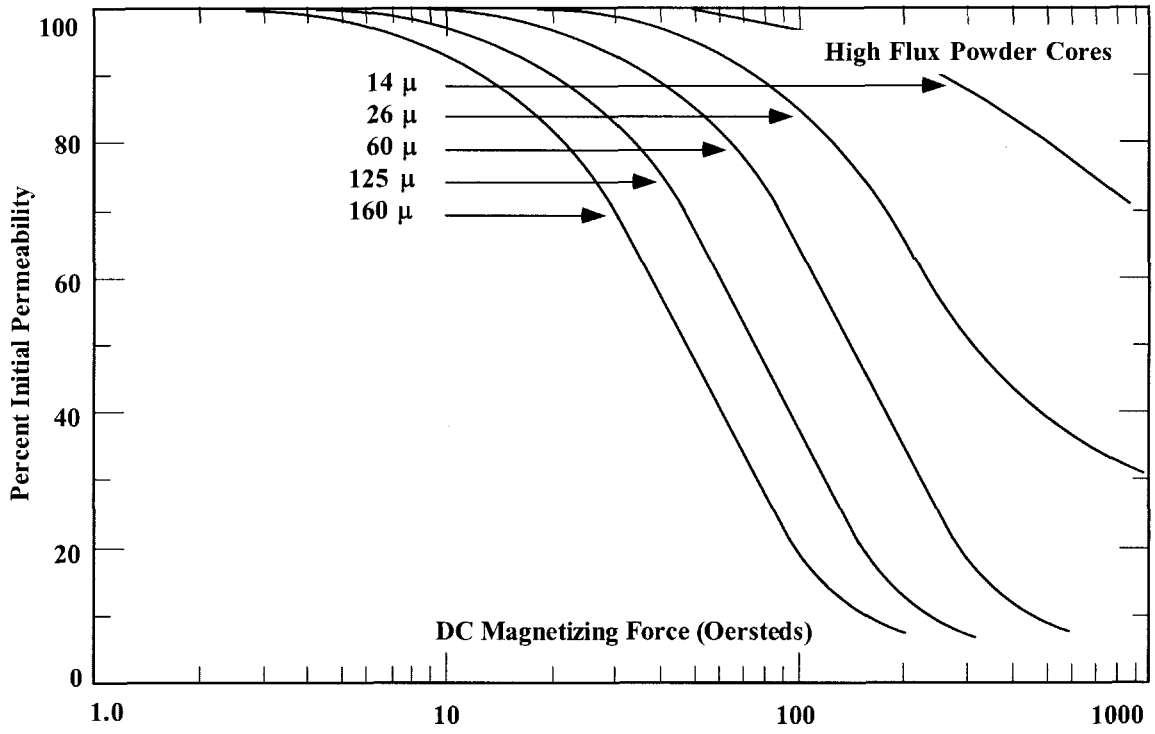

Figure 2-21. Permeability Versus dc Bias for High Flux Powder Cores.

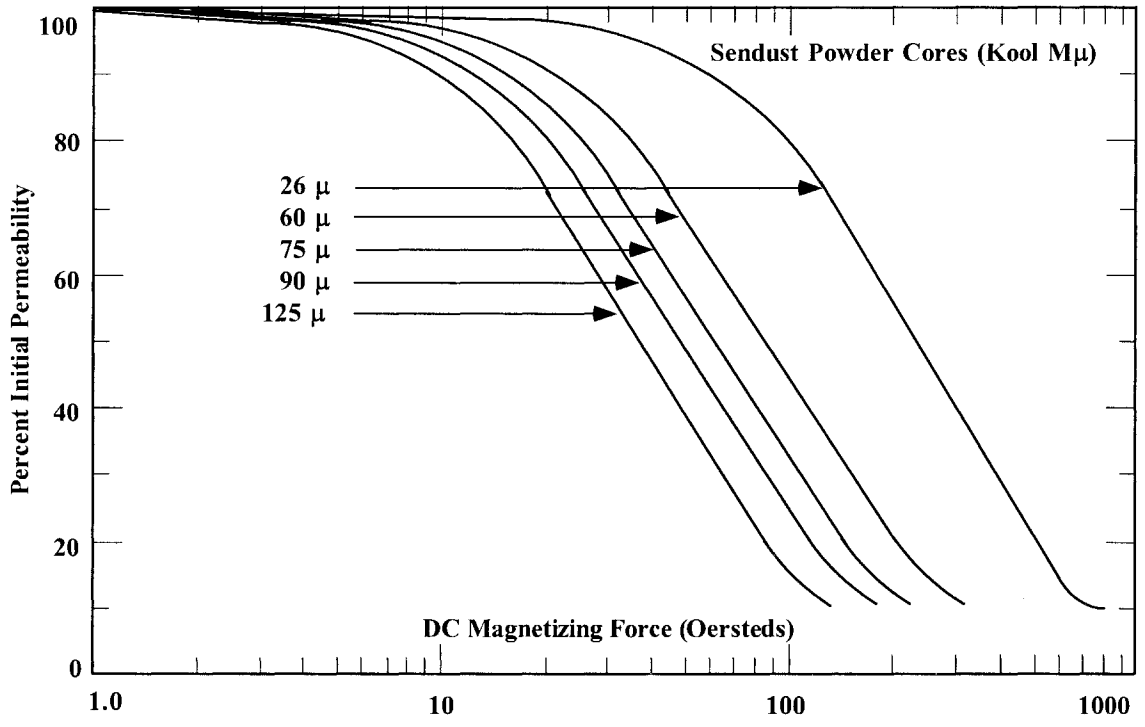

Figure 2-22. Permeability Versus dc Bias for Sendust Powder Cores.

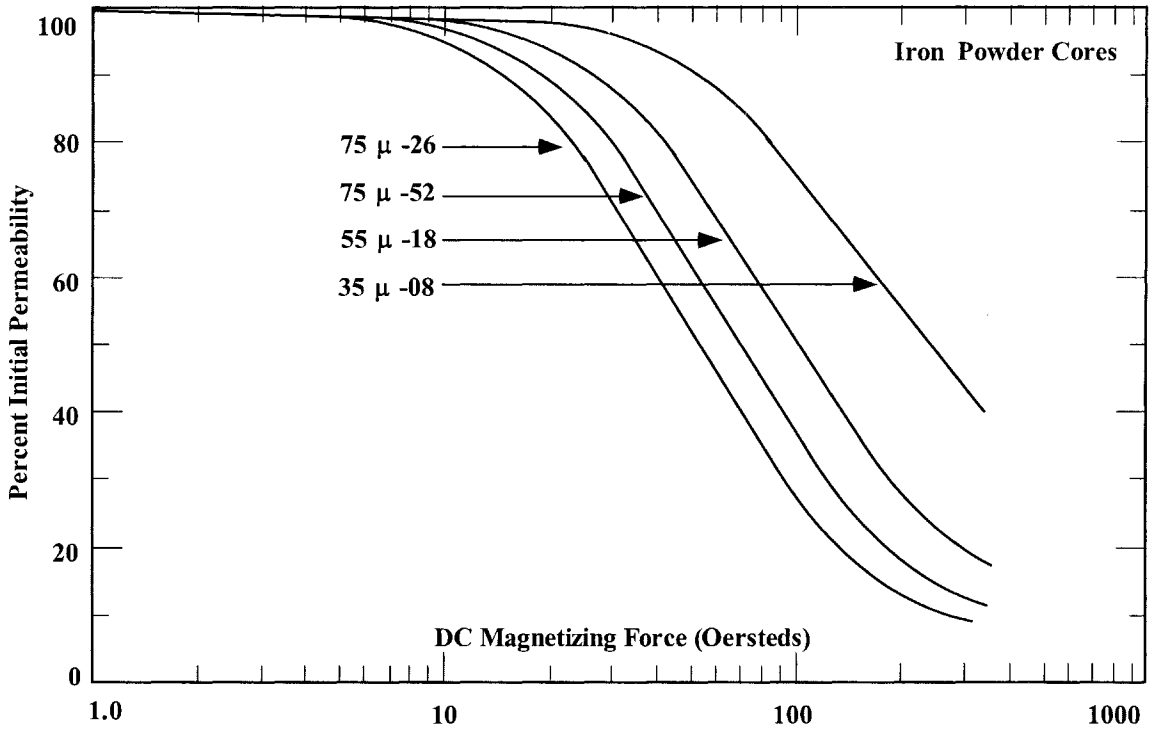

Figure 2-23. Permeability Versus dc Bias for Iron Powder Cores.

Core Loss

The designer of power magnetic components, such as transformer and inductors, requires specific knowledge about the electrical and magnetic properties of the magnetic materials used in these components. There are two magnetic properties that are of interest, the dc and the ac. The dc B-H hysteresis loop is a very useful guide for comparing the different types of magnetic materials. It is the ac magnetic properties that are of interest to the design engineer. One of the most important ac properties is the core loss. The ac core loss is a function of the magnetic material, magnetic material thickness, magnetic flux density B_{ac}, frequency f, and operating temperature. Thus, the choice of the magnetic material is based upon achieving the best characteristic using the standard trade-off such as cost, size, and performance.

All manufacturers do not use the same units when describing their core loss. The user should be aware of the different core loss units when comparing different magnetic materials. A typical core loss graph is shown in Figure 2-24. The vertical scale is core loss, and the horizontal scale is flux density. The core loss data is plotted at different frequencies, as shown in Figure 2-24.

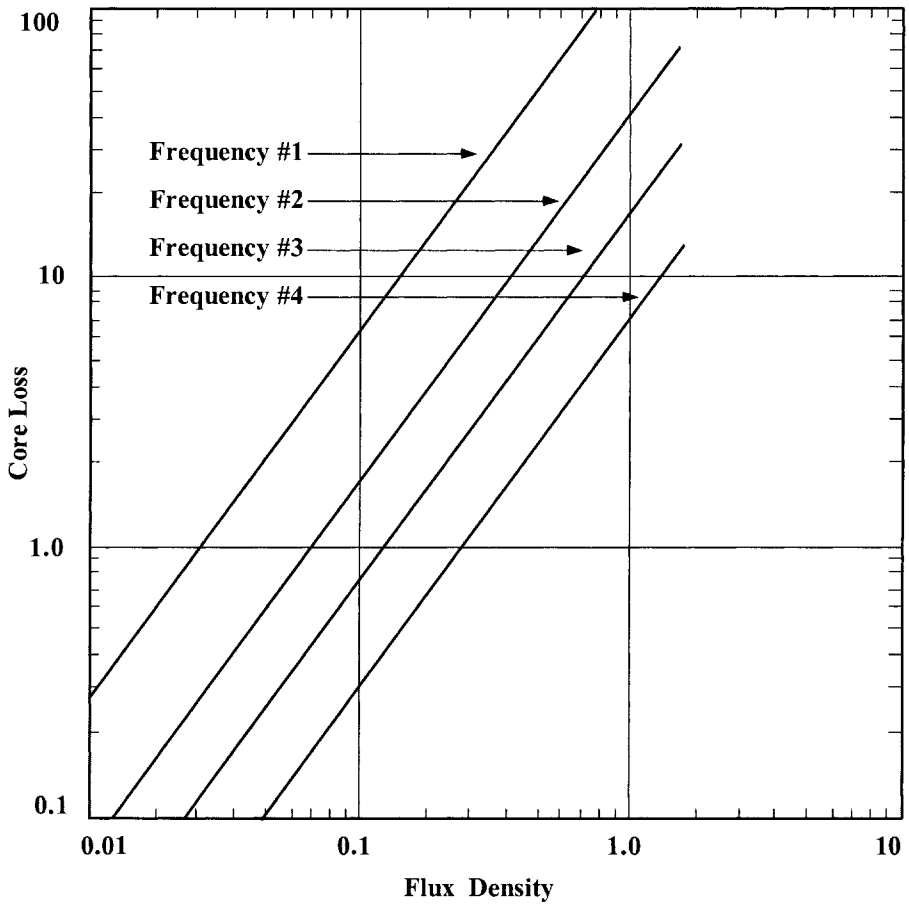

Figure 2-24. Typical Graph for Plotting Core Loss at Different Frequencies.

Vertical Scale

Here is a list of core loss units used by manufacturers:

1. watts per pound
2. watts per kilogram
3. milliwatts per gram
4. milliwatts per cubic centimeter (cm^3)

Horizontal Scale

Here is a list of flux density units used by manufacturers:

1. gauss
2. kilogauss
3. tesla
4. millitesla

The data can be plotted or presented in either hertz or kilohertz.

Core Loss Equations

Manufacturers are now presenting the core loss in the form of an equation such as:

$$\text{watts/kilogram} = k f^{(m)} B^{(n)} \qquad [2\text{-}2]$$

Here, again, the units will change from one manufacturer to another. In the following tables the manufacturers core loss data has been organized with the same units for all core losses. The data was modified to put the data in metric units, gauss to tesla and, watts per pound to watts per kilogram. The coefficients for Magnetics Inc. molypermalloy powder cores, (MPP), using Equation [2-2] are shown in Table 2-9. The coefficients for Magnetics Inc. High Flux powder cores, (HF), using Equation [2-2] are shown in Table 2-10. The coefficients for Magnetics Inc. Sendust powder cores, (Kool-Mμ), using Equation [2-2] are shown in Table 2-11. The coefficients for iron alloy materials using Equation [2-2] are shown in Table 2-12.

Table 2-9. Core Loss Coefficients for MPP Powder Cores.

Core Loss Equation Factors				
Magnetics MPP Powder Cores				
Material	Permeability μ	Coefficient k	Coefficient (m)	Coefficient (n)
MPP	14	0.005980	1.320	2.210
MPP	26	0.001190	1.410	2.180
MPP	60	0.000788	1.410	2.240
MPP	125	0.001780	1.400	2.310
MPP	147-160-173	0.000489	1.500	2.250
MPP	200-300	0.000250	1.640	2.270
MPP	550	0.001320	1.590	2.360

Table 2-10. Core Loss Coefficients for High Flux Powder Cores.

Core Loss Equation Factors				
Magnetics HF Powder Cores				
Material	Permeability μ	Coefficient k	Coefficient (m)	Coefficient (n)
High Flux	14	$4.8667(10^{-7})$	1.26	2.52
High Flux	26	$3.0702(10^{-7})$	1.25	2.55
High Flux	60	$2.0304(10^{-7})$	1.23	2.56
High Flux	125	$1.1627(10^{-7})$	1.32	2.59
High Flux	147	$2.3209(10^{-7})$	1.41	2.56
High Flux	160	$2.3209(10^{-7})$	1.41	2.56

Table 2-11. Core Loss Coefficients for Sendust Powder Cores.

Core Loss Equation Factors				
Magnetics Kool-Mμ Powder Cores				
Material	Permeability μ	Coefficient k	Coefficient (m)	Coefficient (n)
Sendust	26	0.000693		
Sendust	60	0.000634		
Sendust	75	0.000620	1.460	2.000
Sendust	90	0.000614		
Sendust	125	0.000596		

Table 2-12. Core Loss Coefficients for Iron Alloy Cores.

Core Loss Equation Factors					
Iron Alloy					
Material	Thickness mil's	Frequency Range	Coefficient k	Coefficient (m)	Coefficient (n)
50/50 Ni-Fe	1.00		0.0028100	1.210	1.380
	2.00		0.0005590	1.410	1.270
	4.00		0.0006180	1.480	1.440
Supermendur	2.00		0.0236000	1.050	1.300
	4.00	400 Hz	0.0056400	1.270	1.360
Permalloy 80	1.00		0.0000774	1.500	1.800
	2.00		0.0001650	1.410	1.770
	4.00		0.0002410	1.540	1.990
Supermalloy	1.00		0.0002460	1.350	1.910
	2.00		0.0001790	1.480	2.150
	4.00		0.0000936	1.660	2.060
Silicon	1.00		0.0593000	0.993	1.740
	2.00		0.0059700	1.260	1.730
	4.00		0.0035700	1.320	1.710
	12.00		0.0014900	1.550	1.870
	14.00		0.0005570	1.680	1.860
	24 M27 non-or	50-60 Hz	0.0386000	1.000	2.092

The coefficients for amorphous materials, using Equation [2-2] are shown in Table 2-13. The coefficients for Magnetics ferrite materials, using Equation [2-2] are shown in Table 2-14. The coefficients for Micrometals iron powder materials, using Equation [2-3] are shown in Table 2-15.

$$\text{watts/kilogram} = k\left(\frac{f B_{ac}^{3}\left(10^{9}\right)}{(a)+681(b)B_{ac}^{0.7}+2.512\left(10^{6}\right)(c)B_{ac}^{1.35}}\right)+100(d)f^{2}B_{ac}^{2} \quad [2.3]$$

Table 2-13. Core Loss Coefficients for Amorphous Materials.

Core Loss Equation Factors				
Amorphous				
Material	Thickness mils	Coefficient k	Coefficient (m)	Coefficient (n)
2605SC	0.80	$8.79(10^{-6})$	1.730	2.230
2714A	0.80	10.1(10-6)	1.550	1.670
Vitroperm 500	0.80	0.864(10-6)	1.834	2.112

Table 2-14. Core Loss Coefficients for Magnetics Ferrites Materials.

Core Loss Equation Factors				
Magnetic's Ferrite Core Materials				
Material	Frequency Range	Coefficient k	Coefficient (m)	Coefficient (n)
K	f < 500kHz	$2.524(10^{-4})$	1.60	3.15
K	500kHz <= f < 1.0 MHz	$8.147(10^{-8})$	2.19	3.10
K	f => 1.0 MHz	$1.465(10^{-19})$	4.13	2.98
R	f < 100kHz	$5.597(10^{-4})$	1.43	2.85
R	100kHz <= f < 500kHz	$4.316(10^{-5})$	1.64	2.68
R	f => 500kHz	$1.678(10^{-6})$	1.84	2.28
P	f < 100kHz	$1.983(10^{-3})$	1.36	2.86
P	100kHz <= f < 500kHz	$4.855(10^{-5})$	1.63	2.62
P	f => 500kHz	$2.068(10^{-15})$	3.47	2.54
F	f =< 10kHz	$7.698(10^{-2})$	1.06	2.85
F	10kHz < f < 100kHz	$4.724(10^{-5})$	1.72	2.66
F	100kHz <= f < 500kHz	$5.983(10^{-5})$	1.66	2.68
F	f => 500kHz	$1.173(10^{-6})$	1.88	2.29
J	f =< 20kHz	$1.091(10^{-3})$	1.39	2.50
J	f > 20kHz	$1.658(10^{-8})$	2.42	2.50
W	f =< 20kHz	$4.194(10^{-3})$	1.26	2.60
W	f > 20kHz	$3.638(10^{-8})$	2.32	2.62
H	f =< 20kHz	$1.698(10^{-4})$	1.50	2.25
H	f > 20kHz	$5.3720(10^{-5})$	1.62	2.15

Table 2-15. Core Loss Coefficients for Iron Powder Cores.

Core Loss Equation Factors					
Micrometals Iron Powder Cores					
Material	Permeability μ	Coefficient (a)	Coefficient (b)	Coefficient (c)	Coefficient (d)
Mix-08	35	0.01235	0.8202	1.4694	$3.85(10^{-7})$
Mix-18	55	0.00528	0.7079	1.4921	$4.70(10^{-7})$
Mix-26	75	0.00700	0.4858	3.3408	$2.71(10^{-6})$
Mix-52	75	0.00700	0.4858	3.6925	$9.86(10^{-7})$

Selection of Magnetic Materials

Transformers used in static inverters, converters, and transformer-rectifier, (T-R), supplies, intended for aerospace and electronics industry power applications, are usually square loop tape, toroidal design. The design of reliable, efficient, and lightweight devices for this use has been seriously hampered by the lack of engineering data, describing the behavior of both the commonly used and more exotic core materials, with higher-frequency square wave excitation.

A program was carried out at the Jet Propulsion Laboratory, JPL, to develop these data from measurements of the dynamic B-H loop characteristics of the tape core materials presently available from various industry sources. Cores were produced in both toroidal and C forms, and were tested in both ungapped (uncut) and gapped (cut) configurations. This section describes the results of that investigation.

Typical Operation

A transformer used for inverters, converters, and transformer-rectifier suppliers operates from a power bus, which could be dc or ac. In some power applications, a commonly used circuit is a driven transistor switch arrangement, such as that shown in Figure 2.25.

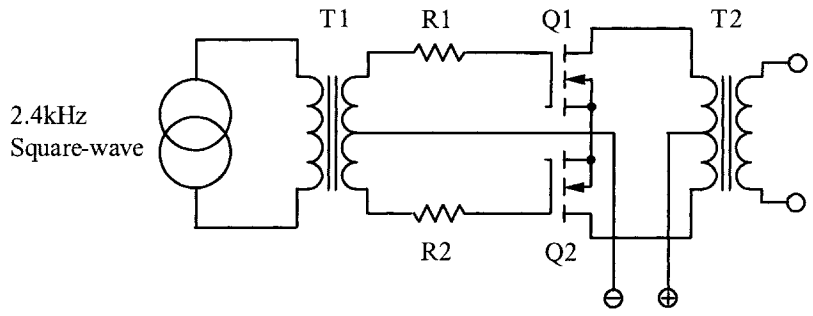

Figure 2-25. Typical Driven Power MOSFET Inverter.

One important consideration affecting the design of suitable transformers is that care must be taken to ensure that operation involves balance drive to the transformer primary. In the absence balance drive, a net dc current will flow in the transformer primary, which causes the core to saturate easily during alternate half-cycles. A saturated core cannot support the applied voltage, limited mainly by its on resistance. The resulting high current, in conjunction with the transformer leakage inductance, results in a high-voltage spike during the switching sequence, which could be destructive to the power MOSFET. To provide balanced drive, it is necessary to exactly match the MOSFETs for $R_{DS(on)}$. But, this is not always sufficiently effective. Also, exact matching of the MOSFETs is a major problem in a practical sense.

Material Characteristics

Many available core materials approximate the ideal square loop characteristic, illustrated by the B-H curve, as shown in Figure 2-26. Representative, dc B-H loops for commonly available core materials, are shown in Figure 2-27. Other characteristics are tabulated in Table 2-16.

Many articles have been written about inverter and converter transformer design. Usually, authors' recommendations represent a compromise among material characteristics, such as those tabulated in Table 2-16, and displayed in Figure 2-27. These data are typical of commercially available core materials that are suitable for the particular application.

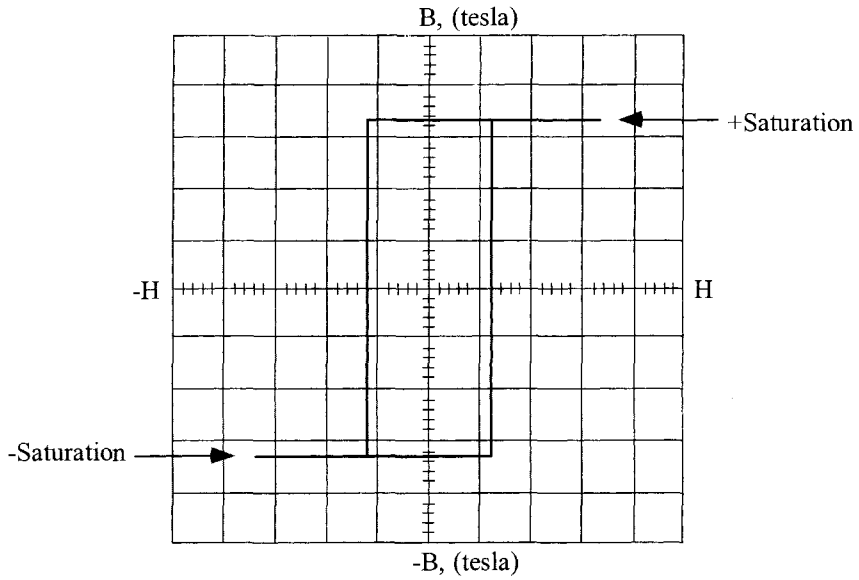

Figure 2-26. Ideal Square B-H Loop.

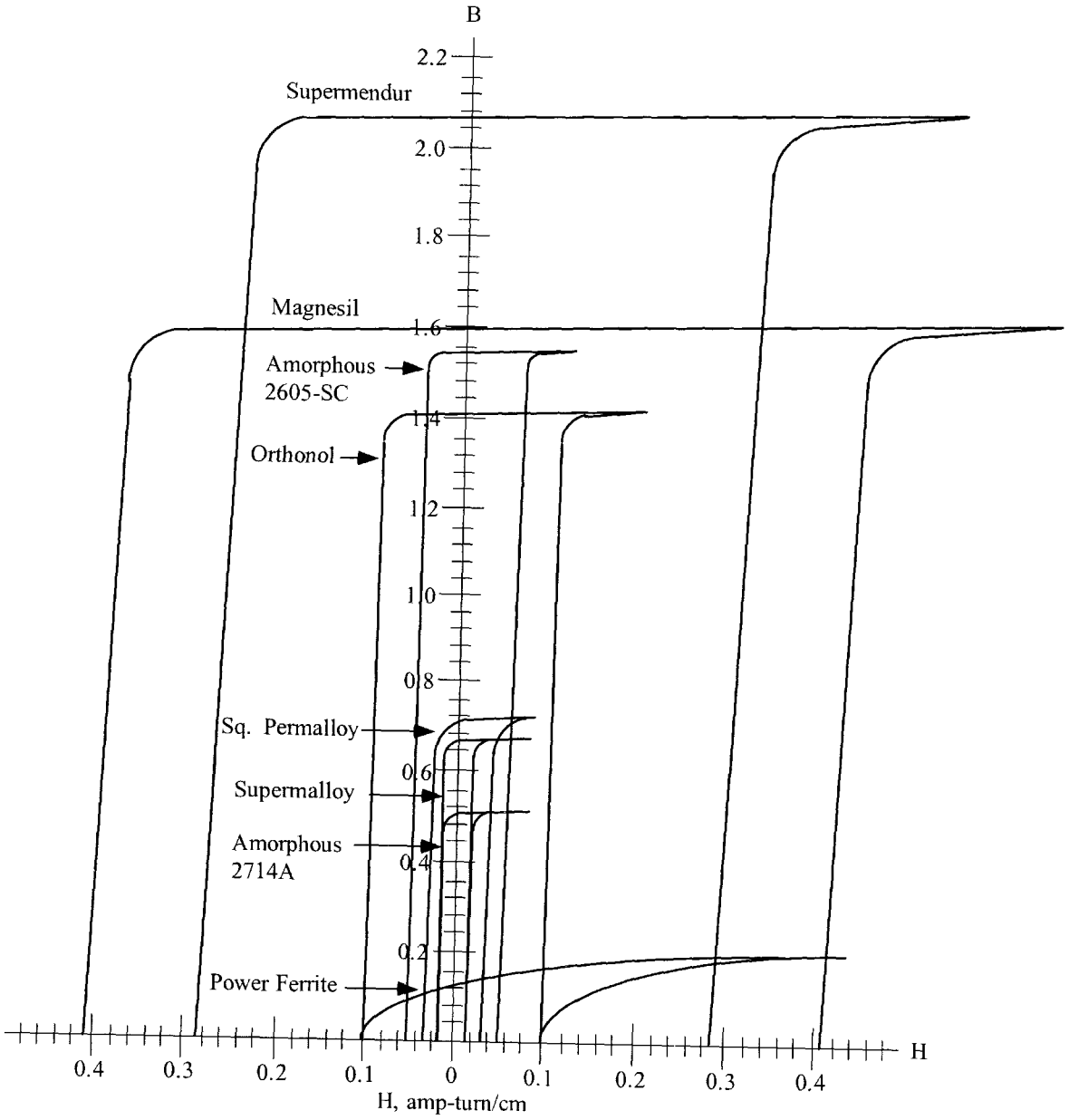

Figure 2-27. Typical dc B-H Loops of Magnetic Materials.

As can be seen, the material that provides the highest flux density (supermendur) would result in the smallest component size, and this would influence the choice if size were the most important consideration. The ferrite material, (see the ferrite curve in Figure 2-27), has the lowest flux density. This results in the largest transformer. Magnetic materials selected for transformers or inductors cannot be chosen by flux alone. There are other parameters, such as frequency and core configuration that must be taken into consideration.

Table 2-16. Magnetic Core Material Characteristics.

Magnetic Core Material Characteristics						
Material Name	Composition	Initial Permeability μ_i	Flux Density Tesla B_s	Curie Temperature °C	dc, Coercive Force, Hc Oersteds	Density grams/cm^3 δ
Magnesil	3% Si 97% Fe	1.5 K	1.5-1.8	750	0.4-0.6	7.3
Supermendur*	49% Co 49% Fe 2% V	0.8 K	1.9-2.2	940	0.15-0.35	8.15
Orthonol	50% Ni 50% Fe	2 K	1.42-1.58	500	0.1-0.2	8.24
Sq. Permalloy	79% Ni 17% Fe 4% Mo	12 K-100 K	0.66-0.82	460	0.02-0.04	8.73
Supermalloy	78% Ni 17% Fe 5% Mo	10 K-50 K	0.65-0.82	460	0.003-0.008	8.76
Amorphous 2605-SC	81% Fe 13.5% B 3.5% Fe	3K	1.5-1.6	370	0.03-0.08	7.32
Amorphous 2714A	66% Co 15% Si 4% Fe	20K	0.5-0.58	205	0.008-0.02	7.59
Ferrite	MnZn	0.75-15K	0.3-0.5	100-300	0.04-0.25	4.8
* Field Anneal.						

Usually, inverter transformer design is aimed at the smallest size, the highest efficiency and adequate performance under the widest range of environmental conditions. Unfortunately, the core material that can produce the smallest size has the lowest efficiency, and the highest efficiency materials result in the largest size. Thus, the transformer designer must make tradeoffs between allowable transformer size and the minimum efficiency that can be tolerated. Then, the choice of core material will be based upon achieving the best characteristic on the most critical or important design parameter, and upon acceptable compromises on the other parameters.

After analysis of a number of designs, most engineers choose size rather than efficiency as the most important criterion, and select an intermediate loss factor on core material for their transformers. Consequently, as the frequency is increased, ferrites have become the most popular material.

Magnetic Material Saturation Defined

To standardize the definition of saturation, several unique points on the B-H loop are defined, as shown in Figure 2-28.

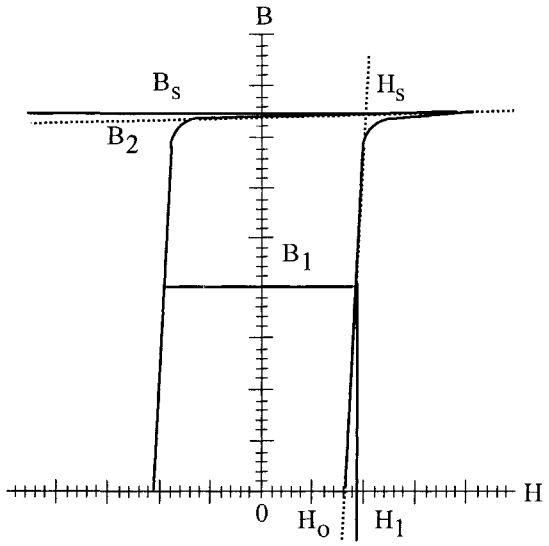

Figure 2-28. Defining the B-H Loop.

The straight line through (H_o, 0) and (H_s, B_s) may be written as:

$$B = \left(\frac{\Delta B}{\Delta H}\right)(H - H_o) \qquad [2\text{-}4]$$

The line through (0, B_2) and (H_s, B_s) has essentially zero slope and may be written as:

$$B = B_2 \approx B_s \qquad [2\text{-}5]$$

Equations [2-1] and [2-2] together define saturation conditions as follows:

$$B_s = \left(\frac{\Delta B}{\Delta H}\right)(H_s - H_o) \qquad [2\text{-}6]$$

Solving Equation [2-3] for H_s yields:

$$H_s = H_o + \frac{B_s}{\mu_o} \qquad [2\text{-}7]$$

Where by definition:

$$\mu_o = \frac{\Delta B}{\Delta H} \qquad [2\text{-}8]$$

By definition, saturation occurs when the peak exciting current (B) is twice the average exciting current (A) as shown in Figure 2-29. Analytically, this means that:

$$H_{pk} = 2H_s \qquad [2\text{-}9]$$

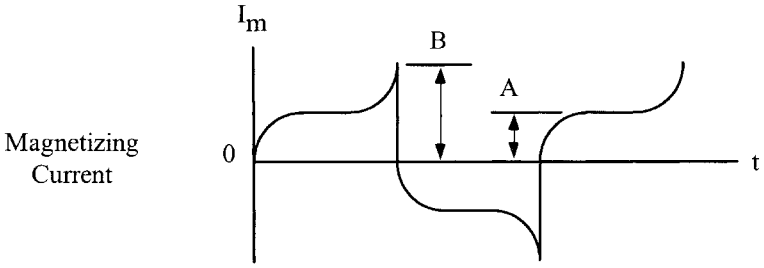

By definition, saturation occurs when B = 2A

Figure 2-29. Defining the Excitation Current.

Solving Equation [2-1] for H_1, we obtain:

$$H_1 = H_o + \frac{B_1}{\mu_o} \qquad [2\text{-}10]$$

To obtain the pre-saturation dc margin (ΔH), Equation [2-4] is subtracted from Equation [2-6]:

$$\Delta H = H_s - H_1 = \left(\frac{B_s - B_1}{\mu_o}\right) \qquad [2\text{-}11]$$

The actual unbalanced dc current must be limited to:

$$I_{dc} \leq \left(\frac{\Delta H(\text{MPL})}{N} \right), \quad \text{[amperes]} \qquad [2\text{-}12]$$

Where, N is the number of turns

MPL is the mean magnetic path length.

Combining Equations [2-7] and [2-8] gives:

$$I_{dc} \leq \left(\frac{(B_s - B_1)(\text{MPL})}{\mu_o N} \right), \quad \text{[amperes]} \qquad [2\text{-}13]$$

As mentioned earlier, in an effort to prevent core saturation, the drive to the switching power MosFet must be symmetrical and the power MosFet on resistance $R_{DS(on)}$ must be matched. The effect of core saturation, using an uncut or ungapped core, is shown in Figure 2-30, which illustrates the effect on the B-H loop transversed with a dc bias. Figure 2-31 shows typical B-H loops of 50-50 nickel-iron material excited from an ac source, with progressively reduced excitation; the vertical scale is 0.4 T/cm. It can be noted that the minor loop remains at one extreme position within the B-H major loop after reduction of excitation. The unfortunate effect of this random minor loop positioning is that, when conduction begins again in the transformer winding after shutdown, the flux swing could begin from the extreme ends rather than from the normal zero axis. The effect of this is to drive the core into saturation, with the production of spikes that can destroy transistors.

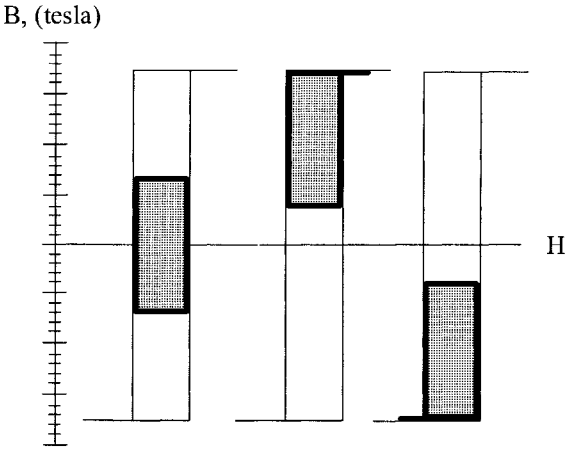

Figure 2-30. B-H Loop with dc Bias.

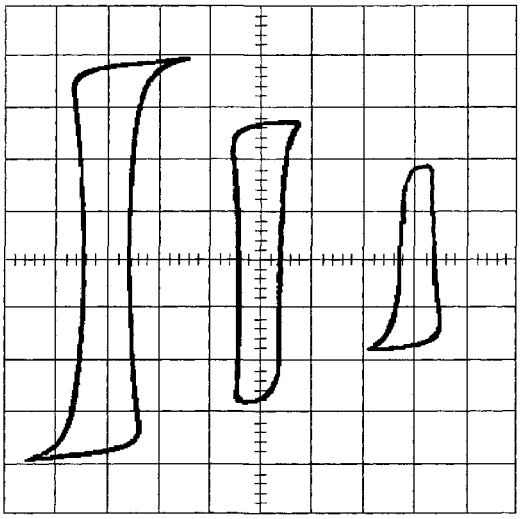

Figure 2-31. Typical Square Loop Material with dc Bias.

Test Conditions

The test fixture, schematically illustrated in Figure 2-32, was built to affect comparison of dynamic B-H loop characteristics of various core materials. Cores were fabricated from various core materials in the basic core configuration, designated No. 52029 for toroidal cores, manufactured by Magnetics Inc. The materials used were those most likely to be of interest to designers of inverter or converter transformers. Test conditions are listed in Table 2-17.

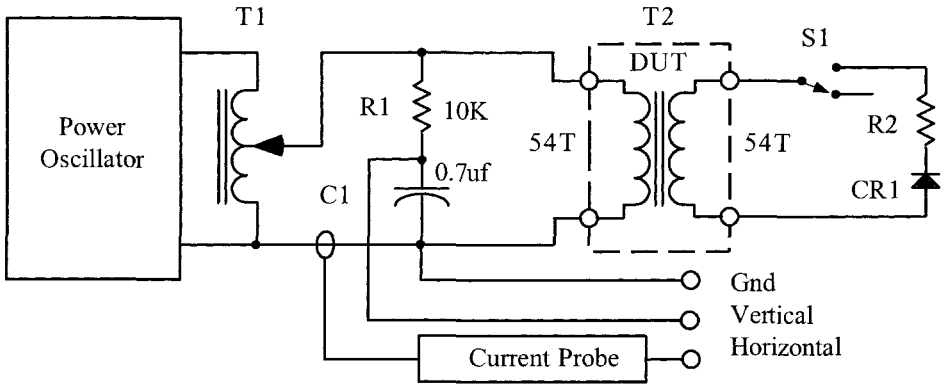

Figure 2-32. B-H Loop with dc Bias.

Winding Data were derived from the following:

$$N = \frac{V\left(10^4\right)}{4.0 B_m f A_c}, \quad \text{[turns]} \quad \text{[2-14]}$$

Table 2-17. Materials and Test Conditions.

Test Conditions					
Core Number*	Trade Name	B_s Tesla	Turns N	Frequency kHz	MPL cm
52029-2A	Orthonol	1.45	54	2.4	9.47
52029-2D	Sq. Permalloy	0.75	54	2.4	9.47
52029-2F	Supermalloy	0.75	54	2.4	9.47
52029-2H	48 Alloy	1.15	54	2.4	9.47
52029-2K	Magnesil	1.6	54	2.4	9.47
*Magnetics toroidal cores.					

The test transformer, represented in Figure 2-32, consists of 54-turn primary and secondary windings, with square wave excitation on the primary. Normally, switch S1 is open. With switch S1 closed, the secondary current is rectified by the diode to produce a dc bias in the secondary winding.

Cores were fabricated from each of the materials by winding a ribbon of the same thickness on a mandrel of a given diameter. Ribbon termination was affected by welding in the conventional manner. The cores were vacuum impregnated, baked, and finished as usual.

Figures 2-33 – 2-36 show the dynamic B-H loops obtained for various core materials. In each of these Figures, switch S1 was in the open position, so there was no dc bias applied to the core and windings.

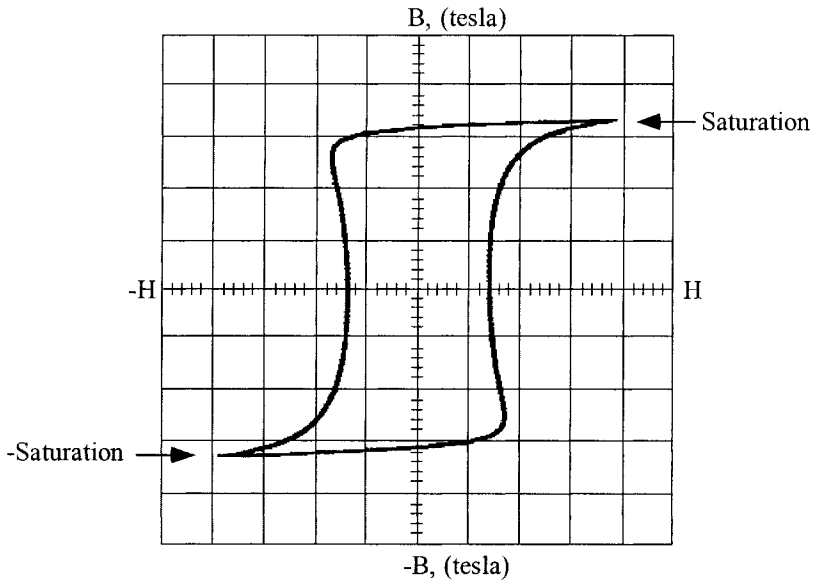

Figure 2-33. Magnesil (K) B-H Loop, B = 0.5 T/cm, H = 100 ma/cm.

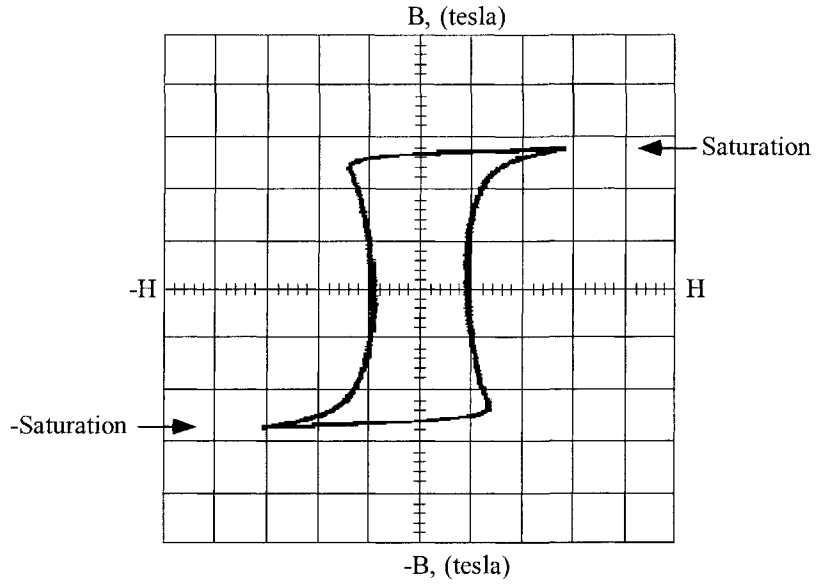

Figure 2-34. Orthonol (2A) B-H Loop, B = 0.5 T/cm, H = 50 ma/cm.

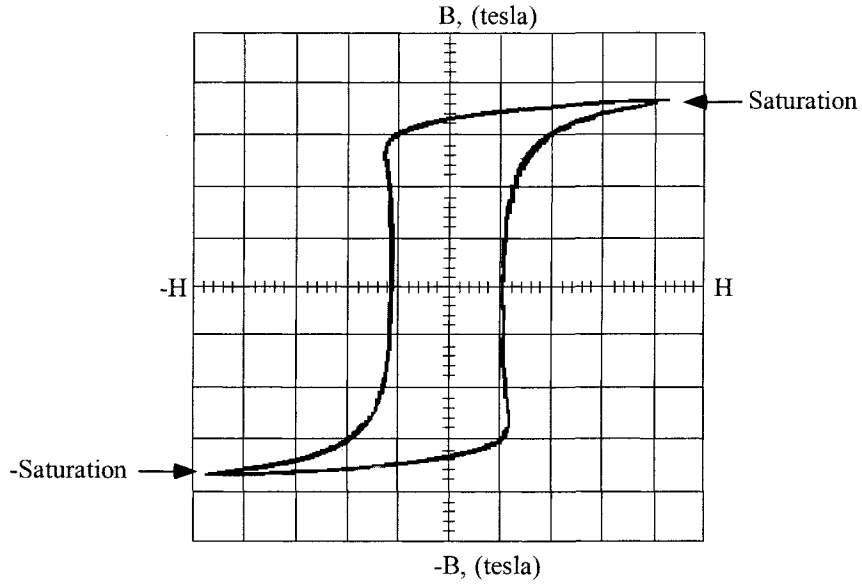

Figure 2-35. Square Permalloy (2D) B-H Loop, B = 0.2 T/cm, H = 20 ma/cm.

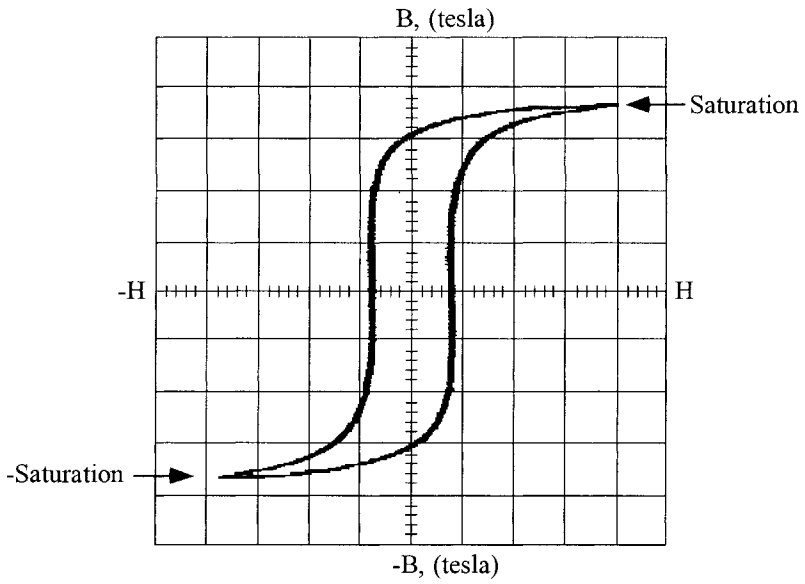

Figure 2-36. Supermalloy (2F) B-H Loop, B = 0.2 T/cm, H = 10 ma/cm.

Figures 2-37 to 2-40 show the dynamic B-H loop patterns obtained for various core materials when the test conditions are included in a sequence, in which S1 was in open condition (A), then in closed condition (B), and then, opened again, in condition (C). It is apparent from this data that, with a small amount of dc bias, the minor dynamic B-H loop can traverse the major B-H loop from saturation to saturation. Note that after the dc bias has been removed, the minor B-H loops remained shifted to one side or the other. Because of the ac coupling of the integrator to the oscilloscope, the photographs in these figures do not present a complete picture of what really happens during the flux swing.

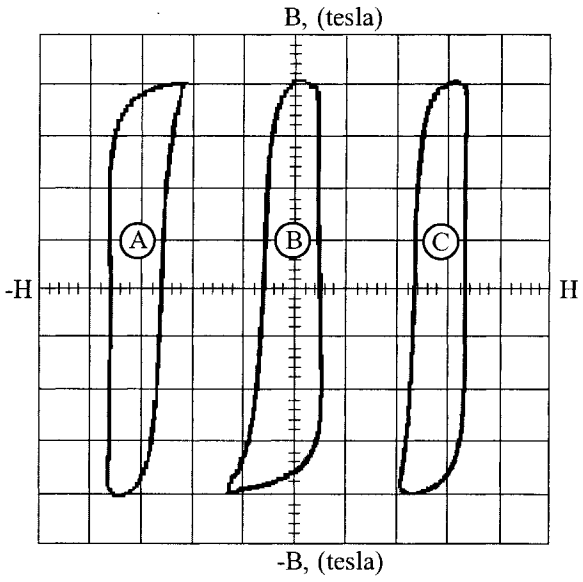

Figure 2-37. Magnesil (2K) B-H Loop, B = 0.3 T/cm, H = 200 ma/cm.

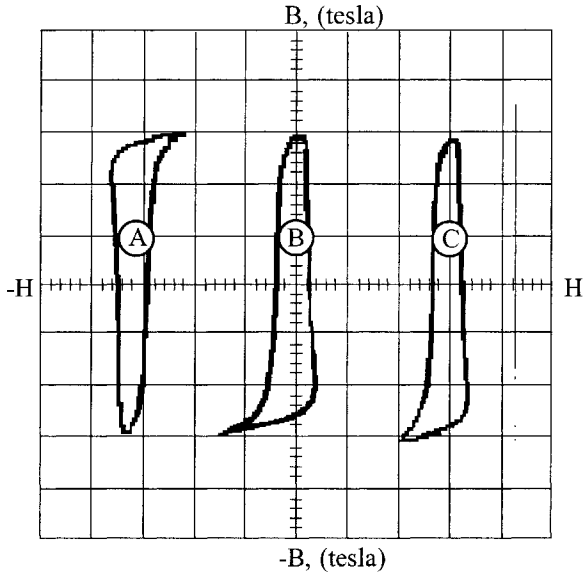

Figure 2-38. Orthonol (2A) B-H Loop, B = 0.2 T/cm, H = 100 ma/cm.

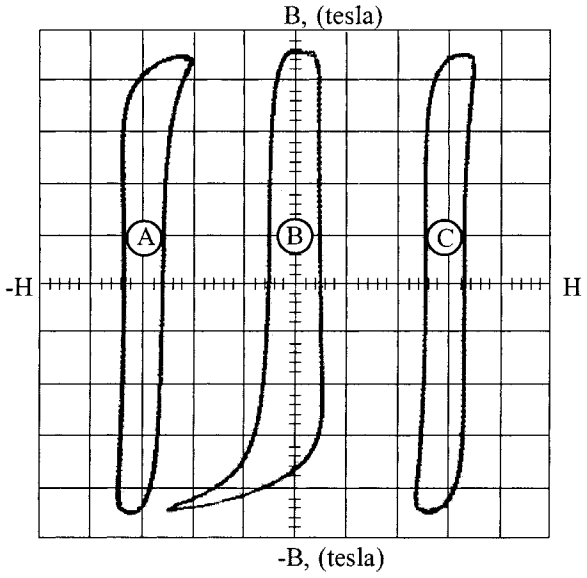

Figure 2-39. Sq. Permalloy (2D) B-H Loop, B = 0.1 T/cm, H = 20 ma/cm.

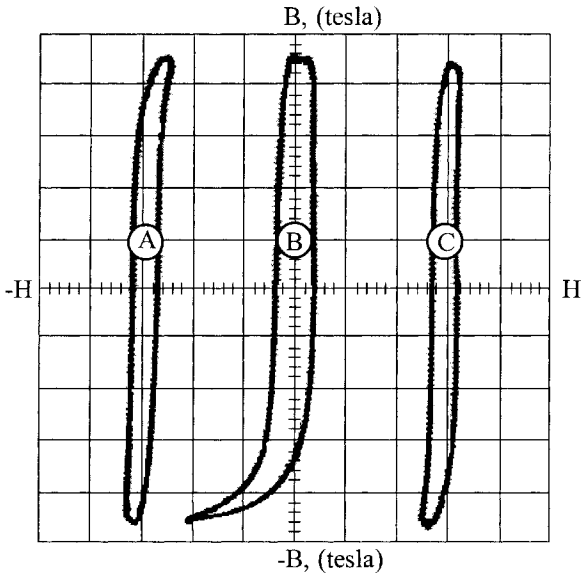

Figure 2-40. Supermalloy (2F) B-H Loop, B = 0.1 T/cm, H = 10 ma/cm.

Magnetic Material Saturation Theory

The domain theory of the nature of magnetism is based on the assumption that all magnetic materials consist of individual molecular magnets. These minute magnets are capable of movement within the material. When a magnetic material is in its unmagnetized state, the individual magnetic particles are arranged at random, and effectively neutralize each other. An example of this is shown in Figure 2-41, where the tiny magnetic particles are arranged in a disorganized manner. (The north poles are represented by the darkened ends of the magnetic particles.) When a material is magnetized, the individual particles are aligned or oriented in a definite direction, as shown in Figure 2-42.

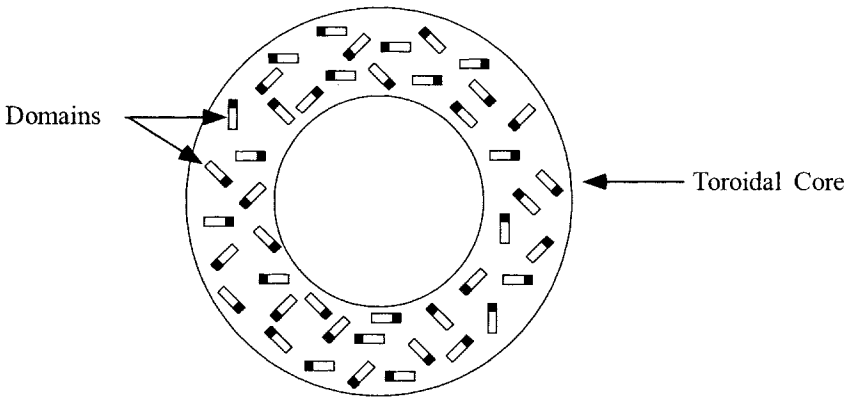

Figure 2-41. Magnetic Domains, Arranged in a Random Manner.

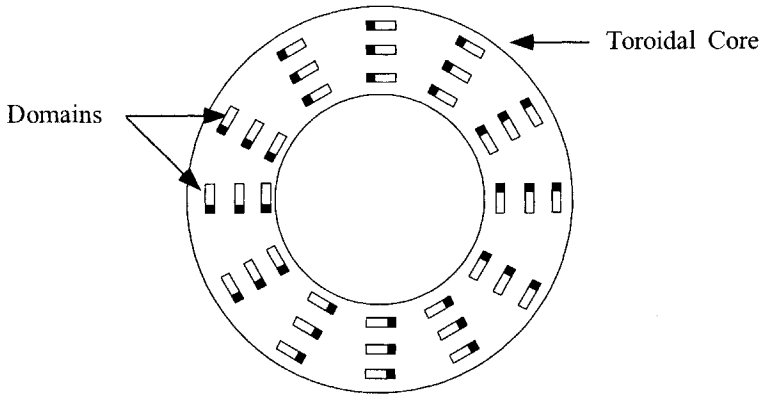

Figure 2-42. Magnetic Domains, Aligned in a Definite Direction.

The degree of magnetization of a material depends on the degree of alignment of the particles. The external magnetizing force can continue to affect the material up to the point of saturation, the point at which essentially all of the domains are lined up in the same direction.

In a typical toroidal core, the effective air gap is less than 10^{-6} cm. Such a gap is negligible in comparison to the ratio of mean length to permeability. If the toroid was subjected to a strong magnetic field (enough to saturate), essentially all of the domains would line up in the same direction. If suddenly the field were removed at B_m, the domains would remain lined up, and be magnetized along that axis. The amount of flux density that remains is called the residual flux, B_r. The result of this effect was shown earlier in Figures 2-37 through 2-40.

Air Gap Effect

An air gap introduced into the core has a powerful demagnetizing effect, resulting in a "shearing over" of the hysteresis loop, and a considerable decrease in permeability of high-permeability materials. Direct current excitation follows the same pattern. However, the core bias is considerably less affected than the magnetization characteristics by the introduction of a small air gap. The magnitude of the air gap effect also depends on the length of the mean magnetic path and on the characteristics of the uncut core. For the same air gap, the decrease in permeability will be less with a greater magnetic flux path, but more pronounced in a high-permeability core with a low coercive force

Effect of Gapping

Figure 2-43 shows a comparison of a typical toroidal core B-H loop, without and with a gap. The gap increases the effective length of the magnetic path. When voltage E is impressed across primary winding, N_p, of a transformer, the resulting current, I_m, will be small because of the highly inductive circuit, as shown in Figure 2-44. For a particular core size, maximum inductance occurs when the air gap is minimum.

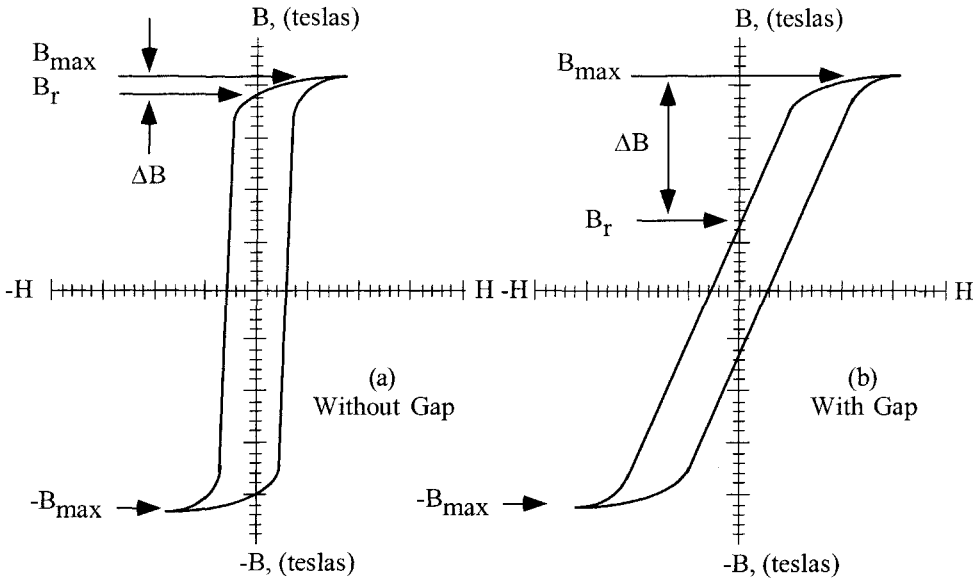

Figure 2-43. Comparing Magnetic Materials with and Without a Gap.

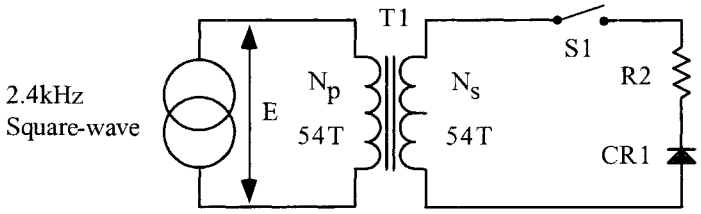

Figure 2-44. Implementing dc Unbalance.

When S1 is closed, an unbalanced dc current flows in the secondary, N_s turns, and the core is subjected to a dc magnetizing force, resulting in a flux density that may be expressed as:

$$B_{dc} = \frac{0.4\pi N_s I_{dc}\left(10^{-4}\right)}{l_g + \frac{\text{MPL}}{\mu_r}}, \quad \text{[tesla]} \quad \text{[2-15]}$$

In converter and inverter design, this dc flux is augmented by the ac flux swing, which is:

$$B_{ac} = \frac{E\left(10^4\right)}{K_f f A_c N}, \quad \text{[tesla]} \quad \text{[2-16]}$$

If the sum of B_{dc} and B_{ac} shifts operations above the maximum operating flux density of the core material, the incremental permeability, (μ_{ac}), is reduced. This condition lowers the impedance and increases the flow

of magnetizing current, I_m. This condition can be remedied by introducing into the core assembly an air gap which causes a decrease in dc magnetization in the core. However, the size of the air gap that can be incorporated has a practical limitation. Since the air gap lowers impedance, it results in increased magnetizing current I_m, which is inductive. The resultant voltage spikes produced by such currents apply a high stress to the switching transistors and may cause failure. This stress can be minimized by tight control of lapping and etching of the gap to keep the gap to a minimum.

From Figure 2-43, it can be seen that the B-H curves depict maximum flux density, B_m, and residual flux, B_r, for ungapped and gapped cores, and that the useful flux swing is designated, ΔB, which is the difference between, B_m and B_r. It will be noted, in Figure 2-43(a), that B_r approaches B_m, but, in Figure 2-43(b), there is a much greater, ΔB, between them. In either case, when excitation voltage is removed at the peak of the excursion of the B-H loop, flux falls to the B_r point. It is apparent that introducing an air gap reduces B_r to a lower level, and increases the useful flux density. Thus, insertion of an air gap in the core eliminates, or markedly reduces, the voltage spikes produced by the leakage inductance, due to the transformer saturation.

Two types of core configurations were investigated in the ungapped and gapped states. Figure 2-45 shows the type of toroidal core that was cut, and Figure 2-46 shows the type of C core that was cut. Toroidal cores are virtually gapless, when conventionally fabricated. To increase the gap, the cores were physically cut in half, and the cut edges were lapped, acid etched to remove cut debris, and banded to form the cores. A minimum air gap, on the order of less than 25 μm, was established.

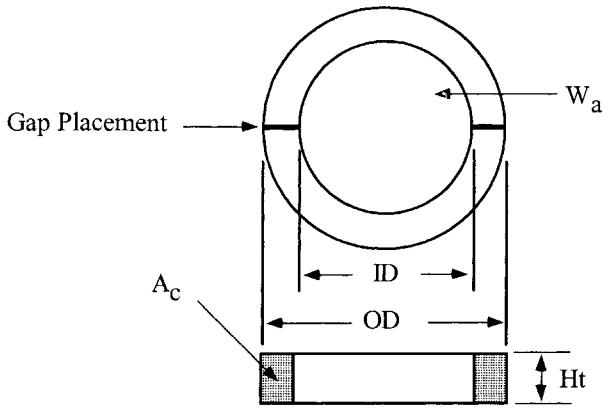

Figure 2-45. Typical cut Toroidal Core.

As will be noted from Figures 2-47 through 2-50, which show the B-H loops of the uncut and cut cores, the results obtained indicated that the effect of gapping was the same for both the C cores and the toroidal cores subjected to testing. It will be noted, however, that gapping of the toroidal cores produced a lowered squareness characteristic for the B-H loop, as shown in Table 2-18. This data was obtained from Figures 2-47 through 2-50. ΔH values extracted from the same figures, as shown in Figure 2-51, are tabulated in Table 2-19.

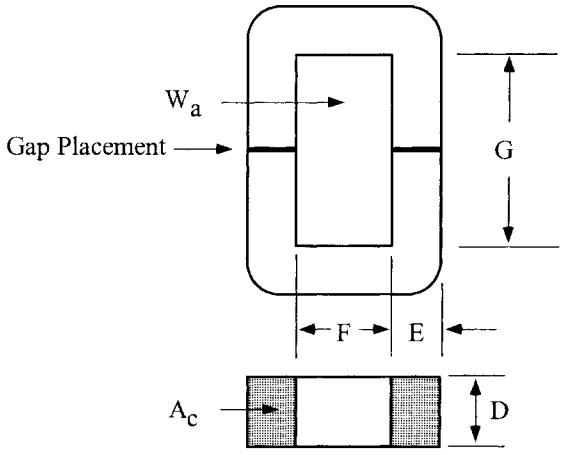

Figure 2-46. Typical Middle Cut C Core.

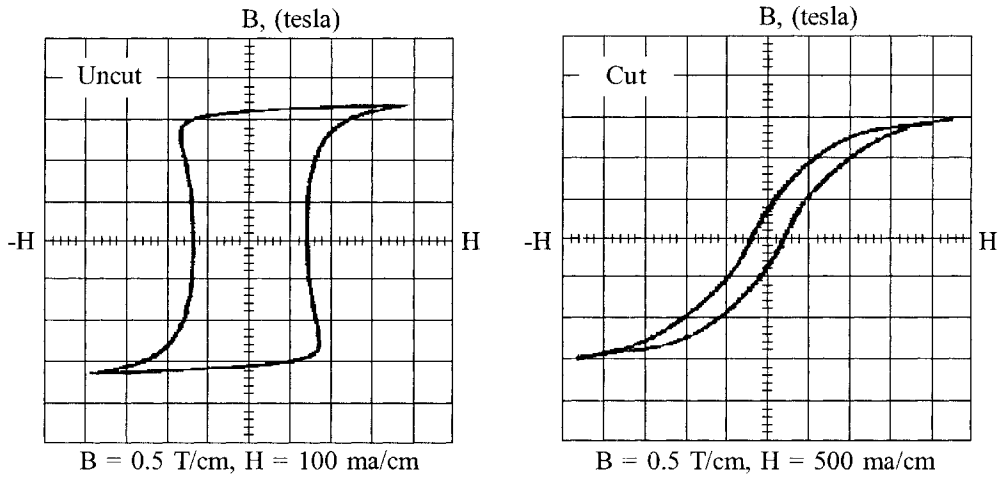

Figure 2-47. Magnesil (K) B-H Loop, Uncut and Cut with Minimum Gap.

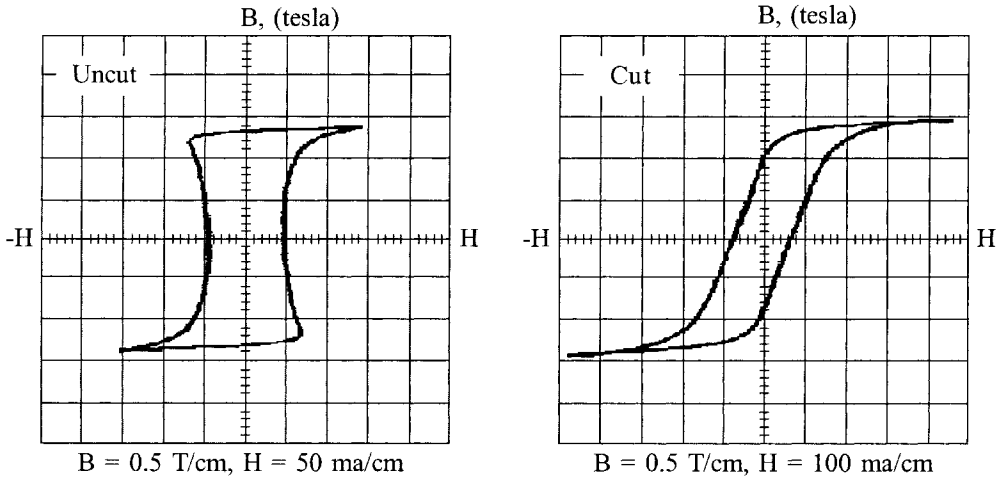

Figure 2-48. Orthonal (A) B-H Loop, Uncut and Cut with Minimum Gap.

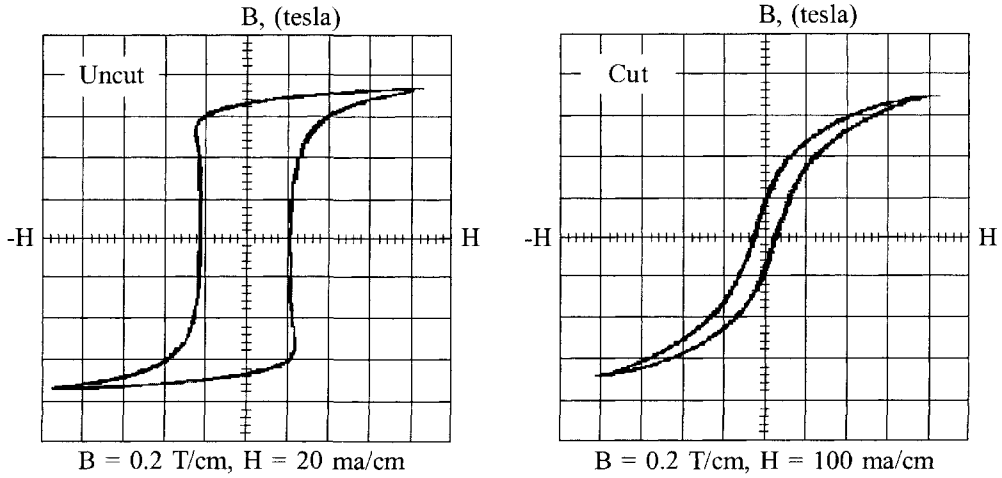

Figure 2-49. Square Permalloy (D) B-H Loop, Uncut and Cut with Minimum Gap.

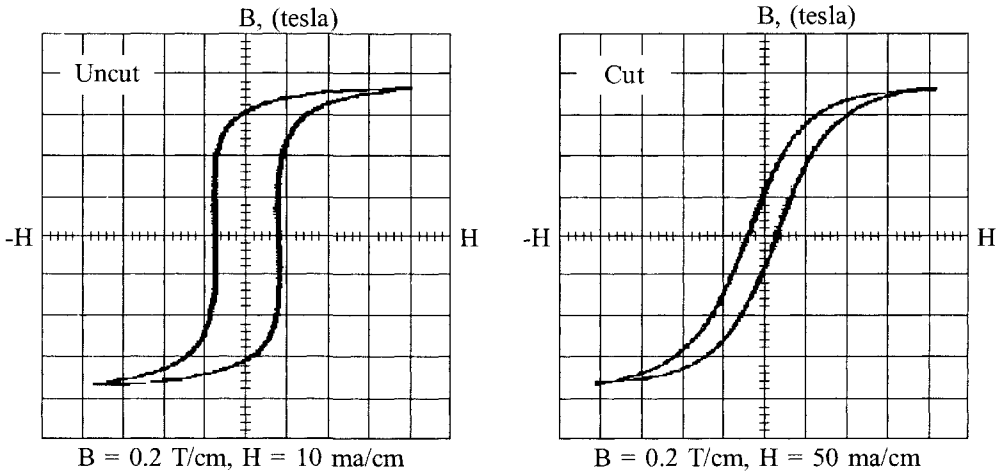

Figure 2-50. Supermalloy (F) B-H Loop, Uncut and Cut with Minimum Gap.

Table 2-18.

Comparing Br/Bm on Uncut and Cut Cores.					
Core Number*	Trade Name	B_s Tesla	Turns N	Uncut B_r/B_m	Cut B_r/B_m
52029-2A	Orthonol	1.45	54	0.96	0.62
52029-2D	Sq. Permalloy	0.75	54	0.86	0.21
52029-2F	Superpermalloy	0.75	54	0.81	0.24
52029-2K	Magnesil	1.60	54	0.93	0.22
*Magnetics toroidal cores.					

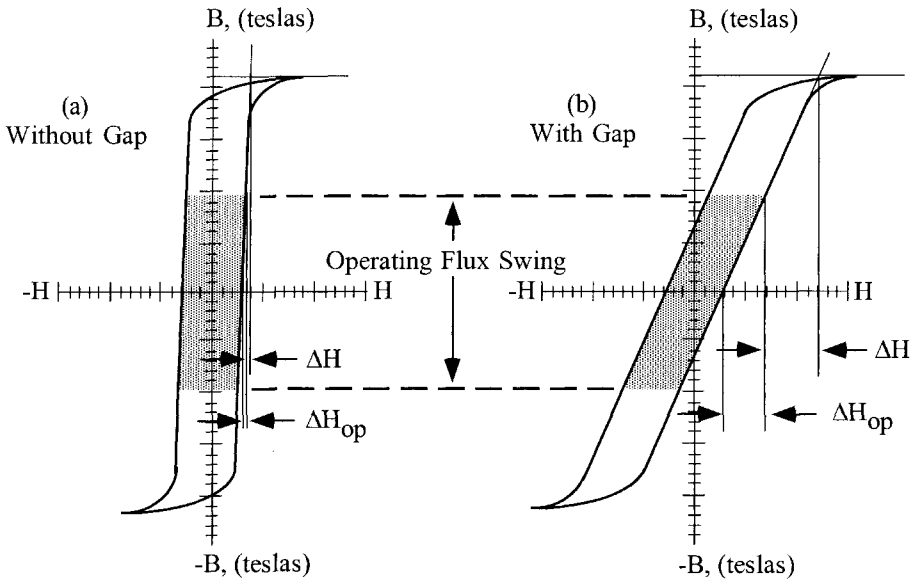

Figure 2-51. Defining ΔH_{op} and ΔH.

Table 2-19. Comparing ΔH and ΔH_{op} on Uncut and Cut Cores.

Comparing ΔH and ΔH_{op} on Uncut and Cut Cores.							
				Amp-turns/cm			
Material	B_m	B_{ac}	B_{dc}	Uncut		Cut	
*Trade Name	Tesla	Tesla	Tesla	ΔH_{op}	ΔH	ΔH_{op}	ΔH
Orthonol	1.44	1.15	0.288	0.0125	0	0.895	0.178
Sq. Permalloy	0.73	0.58	0.146	0.0100	0.005	0.983	0.178
Supermalloy	0.63	0.58	0.136	0.0175	0.005	0.491	0.224
Magnesil	1.54	1.23	0.310	0.0750	0.025	7.150	1.780
*Magnetics Cores.							

A direct comparison of cut and uncut cores was made electrically by means of two different test circuits. The magnetic material used in this branch of the test was Orthonol. The frequency was 2.4 kHz, and the flux density was 0.6 T. The first test circuit, shown in Figure 2-52, was a driven inverter operating into a 30-W load, with the power MOSFETs, operating into and out of saturation. Drive was applied continuously. S1 controls the supply voltage to Q1 and Q2.

With switch S1 closed, transistor Q1 was turned on and allowed to saturate. This applied voltage, E-$V_{DS(on)}$, across the transformer winding. Switch S1 was then opened. Then, the flux in transformer, T2, dropped to the residual flux density, B_r. Switch S1 was closed again. This was done several times in succession to catch the flux in an additive direction. Figures 2-53 and 2-54 show the inrush current measured at the center tap of T2.

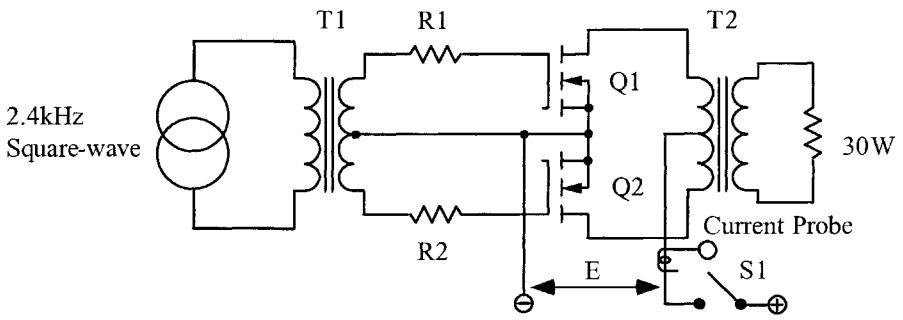

Figure 2-52. Inverter Inrush Current Test Fixture.

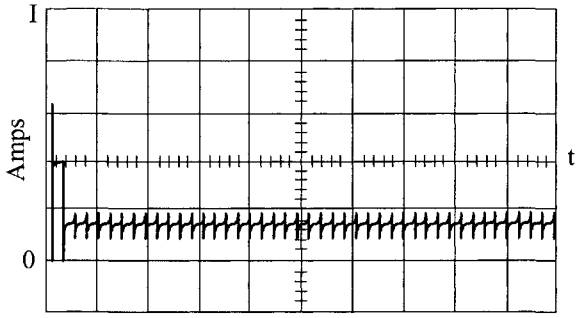

Figure 2-53. Typical Inrush Current of a Uncut Core in a Driven Inverter.

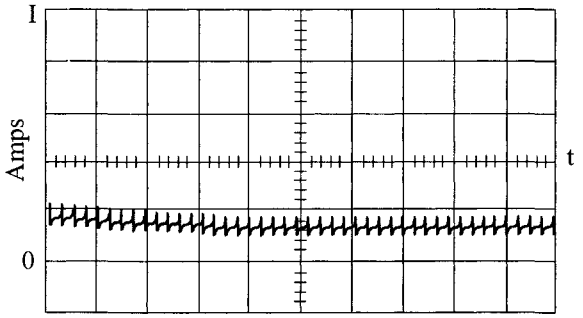

Figure 2-54. Resulting Inrush Current using a Cut Core.

It will be noted, in Figure 2-53, that the uncut core saturated, and the inrush current was limited only by circuit resistance and power, MOSFETs $R_{DS(on)}$. Figure 2-54 shows that saturation did not occur in the case of the cut core. Thus, the high inrush current and transistor stress were virtually eliminated.

The second test circuit arrangement is shown in Figure 2-55. The purpose of this test was to excite a transformer and measure the inrush current, using a current probe. A square wave power oscillator was used to excite transformer, T2. Switch, S1, was opened and closed several times to catch the flux in an additive direction. Figures 2-56 and 2-57 show inrush current for an uncut and cut core, respectively.

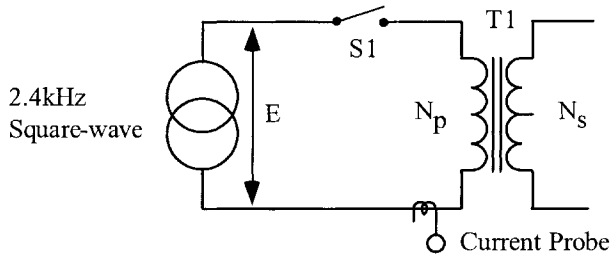

Figure 2-55. Transformer Rectifier Inrush Current Measurement.

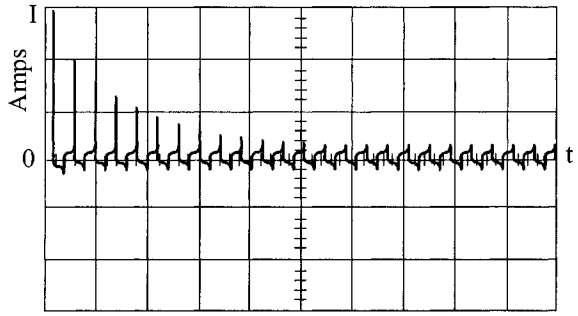

Figure 2-56. Inrush Current of a Transformer using a Uncut Core.

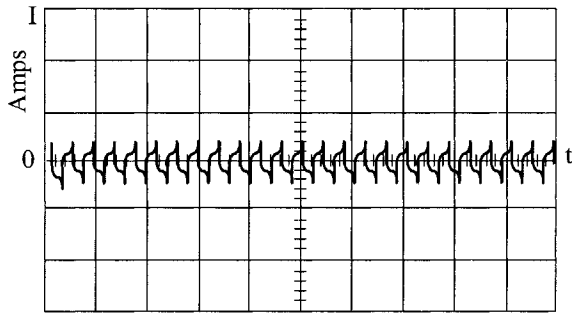

Figure 2-57. Inrush Current of a Transformer using a Cut Core.

A small amount of air gap, less than 25 μm, has a powerful effect on the demagnetizing force, but little effect on the core loss. This small air gap decreases the residual magnetism by "shearing over" the hysteresis loop, which eliminates the problem of the core tending to remain saturated.

A typical example of the merits of the cut core occurred in the checkout of a Mariner spacecraft. During the checkout of a prototype science package, a large (8 A, 200 s) turn-on transient was observed. The normal running current was 0.06 A, fused with a parallel-redundant 1/8-A fuse, as required by the Mariner Mars design philosophy. With the 8-A inrush current, the 1/8-A fuses were easily blown. This did not happen, on every turn-on, but only when the core would "latch up" in the wrong direction for turn-on. Upon inspection, the transformer turned out to be a 50-50 nickel-iron toroid. The design was changed from a toroidal core to a cut core with a 25 μm, air gap. The new design was completely successful in eliminating the 8-A turn-on transient.

Composite Core Configuration

A composite core configuration has been developed for transformers that combine the protective feature of a gapped core with the much lower magnetizing current requirement of an uncut core. The uncut core functions, under normal operating conditions, and the cut core takes over during abnormal conditions to prevent high switching transients and their potentially destructive effect on the transistors.

This configuration is a composite of cut and uncut cores assembled together concentrically, with the uncut core nested within the cut core. The uncut core has high permeability, and thus requires a very small magnetizing current. On the other hand, the cut core has a low permeability and thus requires a much higher magnetization current. The uncut core is designed to operate at a flux density that is sufficient for normal operation of the converter. The uncut core may saturate under the abnormal conditions previously described. The cut core then takes over and supports the applied voltage so that excessive current does not flow. In a sense, it acts like a ballast resistor in some circuits to limit current flow to a safe level.

Figures 2-58 and 2-59 show the magnetization curves for an uncut core and a composite core of the same material at the same flux density. The much lower, B_r characteristic of the composite compared to the uncut core is readily apparent.

The desired features of the composite core can be obtained more economically by using different materials for the cut and uncut portions of the core. It was found that when the design required high nickel (4/79), the cut portion could be low nickel, (50/50), and because low nickel has twice as high a flux density as high nickel, the core was made of 66% high nickel, and 33% low nickel.

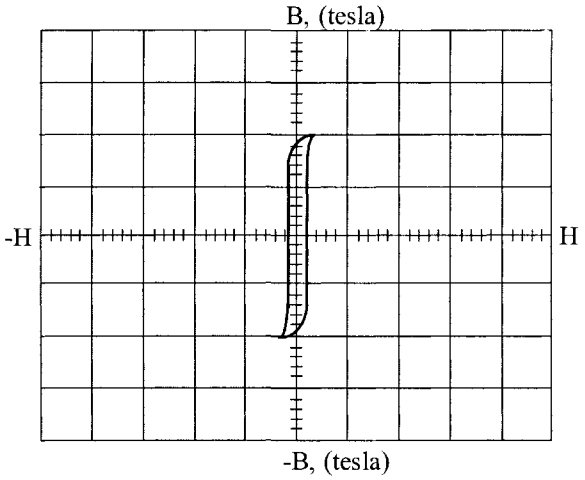

Figure 2-58. Uncut Core Excited at 0.2 T/cm.

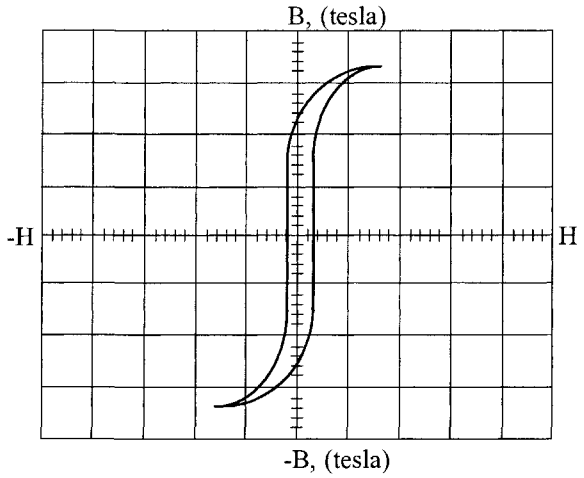

Figure 2-59. Both Cut and Uncut Cores Excited at 0.2 T/cm.

Figure 2-60 shows cut and uncut cores that have been impregnated to bond the ribbon layers together. The uncut core was first trimmed to fit within the inner diameter of the cut core by peeling off a wrap or two of the ribbon steel. The two cores are assembled into a composite core (Figure 2-61, on the right).

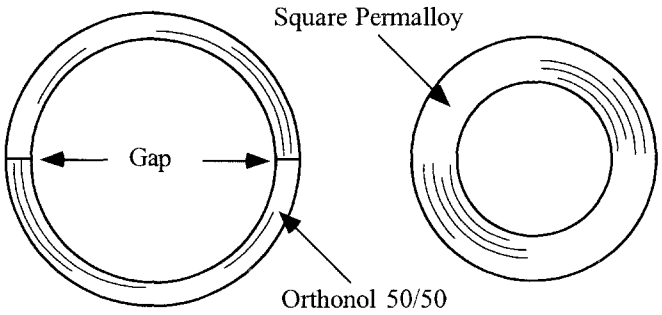

Figure 2-60. Composite Cores Ready for final Assembly.

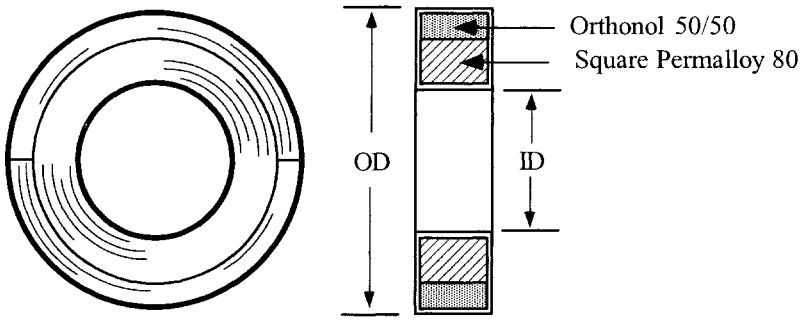

Figure 2-61. Composite Cores Assembled in Final Form.

To ensure uniform characteristics for gapped cores, a gap dimension of 50 μm is recommended, because variations produced by thermal cycling will not affect this gap greatly. In the composite core, the gap is obtained by inserting a sheet of paper Mylar or Kapton film material between the core ends during banding.

The same protective feature can be accomplished in transformers with laminated cores. When laminations are stacked by interleaving them one-by-one, the result will be a minimum air gap, as shown in Figure 2-62 by the squareness of the B-H loop. Shearing over of the B-H loop, or decreasing the residual flux, as shown in Figure 2-63, is accomplished by butt joining half the laminations in the core-cross section, which introduces a small, additional air gap.

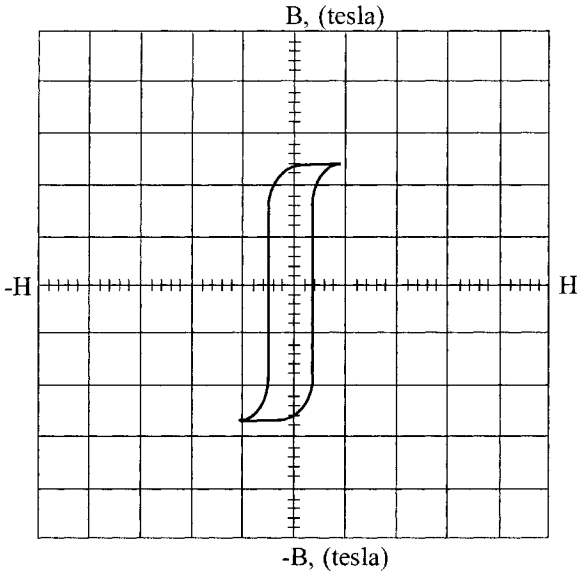

Figure 2-62. B-H Loop with Laminations Stacked 1x1 Interleaved.

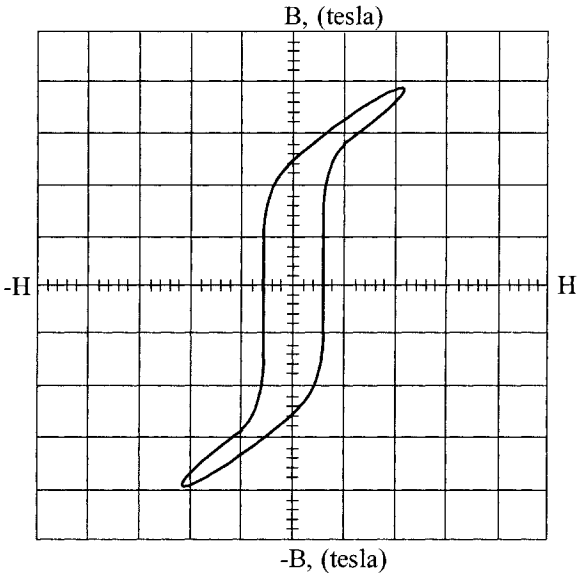

Figure 2-63. B-H Loop with Laminations Stack Half 1x1 and Half Butt Stack.

Table 2-20 is a compiling of composite cores manufactured by Magnetics Inc., alongside their standard dimensional equivalent cores. Also, included in Table 2-20, is the cores' area product, A_p, and the core geometry K_g, which is discussed in Chapter 7.

Table 2-20. Composite Core Listing Along with the Area Product and Core Geometry.

Magnetics Inc. Composite Cores			
Composite Number	Standard Core Number	A_p (cm^4)	K_g (cm^5)
01605-2D	52000	0.0728	0.00105
01754-2D	52002	0.1440	0.00171
01755-2D	52076	0.2850	0.00661
01609-D2	52061	0.3890	0.00744
01756-2D	52106	0.4390	0.00948
01606-2D	52094	0.6030	0.02210
01761-2D	52318	0.7790	0.02600
01757-2D	52029	1.0900	0.02560
01760-2D	52188	1.1520	0.05120
02153-2D	52181	1.2200	0.04070
01758-2D	52032	1.4550	0.04310
01607-2D	52026	2.1800	0.08740
01966-2D	52030	2.3370	0.06350
01759-2D	52038	2.9100	0.14000
01608-2D	52035	4.6760	0.20600
01623-2D	52425	5.2550	0.26200
01624-2D	52169	7.1300	0.41800
A_c = 66% Square Permalloy 4 / 79.			
Ac = 33% Orthonol 50 / 50.			
l_g = 2 mil Kapton.			

Summary

Low-loss tape-wound toroidal core materials, that have a very square hysteresis characteristic, (B-H loop), have been used extensively in the design of spacecraft transformers. Due to the squareness of the B-H loops of these materials, transformers designed with them tend to saturate quite easily. As a result, large voltage and current spikes, which cause undue stress on the electronic circuitry, can occur. Saturation occurs when there is any unbalance in the ac drive to the transformer, or when any dc excitation exists. Also, due to the square characteristic, a high residual flux state, (high B_r), may remain when excitation is removed. Reapplication of excitation in the same direction may cause deep saturation, and an extremely large current spike, limited only by source impedance and transformer winding resistance, can result. This can produce catastrophic failure.

With the introduction of a small, (less than 25 μm), air gap into the core, the problems described above can be avoided while retaining the low-loss properties of the materials. The air gap has the effect of "shearing over" the B-H loop of the material so that the residual flux state is low and the margin between operating,

flux density, and saturation, flux density is high. The air gap thus has a powerful demagnetizing effect upon the square loop materials. Properly designed transformers, using cut toroid or C core square-loop materials, will not saturate upon turn-on, and can tolerate a certain amount of unbalanced drive or dc excitation.

It must be emphasized, however, that because of the nature of the material and the small size of the gap, extreme care and control must be taken in performing the gapping operation. Otherwise, the desired shearing effect will not be achieved, and the low-loss properties will be lost. The cores must be very carefully cut, lapped, and etched to provide smooth, residue-free surfaces. Reassembly must be performed with equal care.